

Many-body theory of current-induced fluorescence in molecular junctions

Upendra Harbola, Jeremy B. Maddox, and Shaul Mukamel

Department of Chemistry, University of California, Irvine, California 92697-2025, USA

(Received 21 August 2005; revised manuscript received 14 November 2005; published 27 February 2006)

Nonequilibrium superoperator Green's function theory is used to calculate the fluorescence signal of molecules induced by currents in scanning tunneling microscope junctions. The spectrum of benzene and its variation with tip position and bias are simulated at the density functional theory level. The formal analogy with laser-induced fluorescence is pointed out. Many-body effects can be accounted for through self-energies and the Keldysh Dyson equations. The sum-over-orbital expressions obtained within density functional theory may not be expressed as an amplitude square. This is due to dephasing effects induced by the many-electron excitations, which act as a bath.

DOI: [10.1103/PhysRevB.73.075211](https://doi.org/10.1103/PhysRevB.73.075211)

PACS number(s): 73.22.-f, 68.37.Ef, 85.65.+h

I. INTRODUCTION

The radiative recombination of electrons and holes injected into molecular materials such as conducting polymers and carbon nanotubes, known as electroluminescence, is an interesting process involving the complex interplay of charge-carrier transport with trapping and disorder.¹ Current induced fluorescence (CIF) forms the basis for many technological applications, e.g., light-emitting diodes. The observation of light emission induced by the electric current in single molecular junctions,² carbon nanotubes,³ and nanowires⁴ is a remarkable recent development. The scanning tunneling microscopy (STM) tip or metal wires allow the control of electron and hole injection into specific positions within a molecule, and ensemble averaging is totally eliminated. Laser-induced fluorescence (LIF), in contrast, is determined by the long-wavelength (dipole) approximation and may not be controlled spatially beyond the ~ 100 nm resolution of near-field techniques. Furthermore, STM is not subjected to optical selection rules and can access a broader range of excited states. Experiments performed on porphyrines and phthalocyanines² have shown a strong variation of the spectrum as the tip is scanned across the molecule.

There have been several studies on the reverse process of photoinduced current in laser-driven molecular wires.⁵⁻⁷ Lehmann *et al.*⁶ have used Floquet formalism to study the quantum rectification properties of a molecular wire ratchet driven by an external laser field in absence of applied dc bias. Charge transfer through a molecular junction under an applied dc bias has been investigated⁸⁻¹⁷ using the nonequilibrium Green's function technique (NEGFT).¹⁸⁻²⁰

In this paper we use the density matrix Liouville space nonequilibrium superoperator Green's function theory²¹⁻²⁵ (NESGFT) to calculate CIF in molecular junctions. In analogy with LIF,²⁶ the fluorescence is expressed in terms of various Liouville space pathways (LSPs). Electron transfer in donor-bridge-acceptor systems has been formulated similarly.^{27,28} The fundamental formal analogy between coherent (tunneling) and Raman signals, and between incoherent (hopping) transport and fluorescence spectra, is most clearly seen when these processes are described using the density matrix in Liouville space.^{26,29} Closed expressions are derived by combining the density matrix approach with

many-body theory. These are recast in terms of nonequilibrium Green's functions which may be computed using standard quantum chemistry techniques.

In the next section, we present the superoperator Liouville space description of conventional LIF. This simpler process will allow us to introduce the formalism and notation, and the necessary time-ordered pathways and Feynman diagrams, setting the stage for computing the current-induced fluorescence in Sec. III. In Sec. IV we present simulations for benzene. We conclude in Sec. V with a discussion.

II. SUPEROPERATOR EXPRESSIONS FOR OPTICALLY INDUCED FLUORESCENCE

We consider a molecule driven by an optical field with a complex envelop $E(t)$ and frequency ω_L . In the rotating wave approximation the molecule-field interaction is given by

$$H_{int} = E(t)B^\dagger \exp(-i\omega_L t) + E^*(t)B \exp(i\omega_L t). \quad (1)$$

$B^\dagger(B)$ are the creation (annihilation) operators for an electronic excitation and $\mu = B + B^\dagger$ is the dipole operator.

The time- (t) and frequency- (ω_S) resolved fluorescence signal is given by the Fourier transform of the two-point time correlation function of the dipole operator^{30,31} (Appendix A)

$$S(\omega_S, \omega_L, t) = \frac{1}{\hbar^2} \int_{-\infty}^{\infty} d\tau e^{-i\omega_S \tau} \langle B^\dagger(t)B(t-\tau) \rangle_D. \quad (2)$$

Here $\langle \dots \rangle_D$ denotes a nonequilibrium average for the *driven* system whose time evolution is in the Heisenberg picture

$$B(t) \equiv \exp\left(\frac{i}{\hbar} \int_{t_0}^t d\tau H_T(\tau)\right) B(t_0) \exp\left(-\frac{i}{\hbar} \int_{t_0}^t d\tau H_T(\tau)\right) \quad (3)$$

where $H_T = H + H_{int}$ is the total Hamiltonian for the molecule (H) and its coupling with the external field. We further define the time evolution in the interaction picture,

$$\tilde{B}(t) \equiv e^{(i/\hbar)H(t-t_0)} B(t_0) e^{-(i/\hbar)H(t-t_0)}. \quad (4)$$

NESGFT is formulated in terms of Liouville space superoperators.^{21,31,32} We shall briefly introduce the basic el-

ements of this technique. With each Hilbert space operator Q , we associate two superoperators, denoted as Q_L (left) and Q_R (right), defined through their left or right action on some Hilbert space operator X ,

$$Q_L X \equiv QX, \quad Q_R X \equiv XQ. \quad (5)$$

We further define the linear combinations of these superoperators $Q^+ \equiv (Q_L + Q_R)/2$ and $Q^- \equiv Q_L - Q_R$. Thus a $+$ ($-$) operation in Liouville space corresponds to an anticommutation (commutation) operation in Hilbert space, $Q^+ X \equiv (QX + XQ)/2$ and $Q^- X \equiv (QX - XQ)$.

A key tool in the following manipulations is the time-ordering operator in Liouville space, \mathcal{T} ; when acting on a product of superoperators, it reorders them so that time increases from right to left. Since the trace of a commutator vanishes, we have

$$\langle \mathcal{T} Q_i^+(t) Q_j^-(t') \rangle = 0, \quad t < t'. \quad (6)$$

One notable advantage of the $+/-$, compared to the L/R representation, is that causal and noncausal quantities appear naturally. $\langle \mathcal{T} Q_i^+(t) Q_j^-(t') \rangle$ is causal while $\langle \mathcal{T} Q_i^-(t) Q_j^+(t') \rangle$ is noncausal, and $\langle \mathcal{T} Q_i^-(t) Q_j^-(t') \rangle$ vanishes identically. From these definitions it follows that

$$\begin{aligned} \langle \mathcal{T} Q_L(t) Q_R^\dagger(t') \rangle &= \theta(t - t') \langle Q_L(t) Q_R^\dagger(t') \rangle + \theta(t' - t) \\ &\quad \times \langle Q_R^\dagger(t') Q_L(t) \rangle \equiv \langle Q^+(t') Q(t) \rangle. \end{aligned} \quad (7)$$

Using Eq. (7), Eq. (2) can be expressed in terms of superoperators,

$$S(\omega_S, \omega_L, t) = \frac{1}{\hbar^2} \int d\tau e^{-i\omega_S \tau} \langle \mathcal{T} B_L(t - \tau) B_R^\dagger(t) \rangle_D. \quad (8)$$

Standard derivations of $S(\omega_S, \omega_L, t)$ use normal ordering of ordinary Hilbert space operators.^{30,33,34} This is not necessary in the present time-ordered form of superoperators.

We next switch to the interaction picture,³²

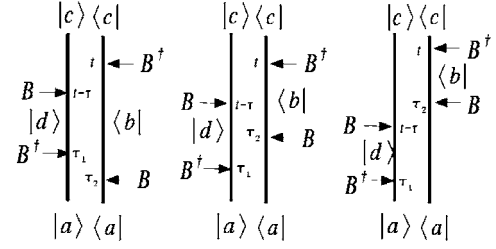
$$\begin{aligned} \langle \mathcal{T} B_L(t - \tau) B_R^\dagger(t) \rangle_D &= \left\langle \mathcal{T} \tilde{B}_L(t - \tau) \tilde{B}_R^\dagger(t) \right. \\ &\quad \times \exp \left(-\frac{i}{\hbar} \int d\tau_1 E(\tau_1) \tilde{B}_-^\dagger(\tau_1) e^{-i\omega_L \tau_1} \right. \\ &\quad \left. \left. - \frac{i}{\hbar} \int d\tau_2 E^*(\tau_2) \tilde{B}_-(\tau_2) e^{i\omega_L \tau_2} \right) \right\rangle. \end{aligned} \quad (9)$$

Here $\langle \dots \rangle$ represents the trace with respect to the density matrix of the material alone. To second order in the external field, which is the lowest order necessary to generate the fluorescence signal, we get

$$\begin{aligned} S(\omega_S, \omega_L, t) &= -\frac{1}{\hbar^4} \int \int \int d\tau d\tau_1 d\tau_2 e^{-i\omega_S \tau - i\omega_L(\tau_1 - \tau_2)} \\ &\quad \times \langle \mathcal{T} \tilde{B}_L(t - \tau) \tilde{B}_R^\dagger(t) \tilde{B}_-^\dagger(\tau_1) \tilde{B}_-(\tau_2) \rangle E(\tau_1) E^*(\tau_2). \end{aligned} \quad (10)$$

Other second-order terms which contain $E(\tau_1)E(\tau_2)$ and

(a) $\tau > 0$



(b) $\tau < 0$

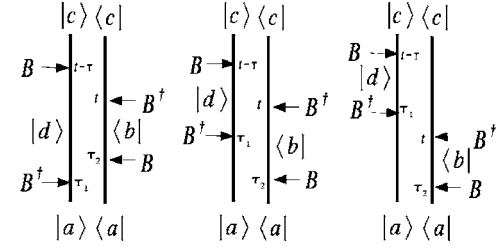


FIG. 1. Double-sided Feynman diagrams corresponding to the six time-ordered interactions that contributing to LIF, Eq. (11). The three processes in (a) for $\tau > 0$ are complex conjugates to $\tau < 0$, shown in (b). Feynman diagrams for CIF from a negatively (positively) charged molecule can be obtained by replacing the two B operators acting at times τ_1 and τ_2 with $\psi_k^\dagger(\psi_k)$ and $\psi_l(\psi_l^\dagger)$, respectively. For CIF, $|a\rangle$, $|b\rangle$, $|c\rangle$, and $|d\rangle$ correspond to states with different number of electrons (see text). Time increases from bottom to top.

$E^*(\tau_1)E^*(\tau_2)$ do not contribute to the signal because their trace vanishes.

Recasting the $+/-$ operators in Eq. (10) in the L/R representation, and keeping in mind that only traces with a pair of left and a pair of right operators survive, Eq. (10) reduces to

$$\begin{aligned} S(\omega_S, \omega_L, t) &= \frac{-1}{\hbar^4} \int \int \int d\tau d\tau_1 d\tau_2 e^{-i\omega_S \tau - i\omega_L(\tau_1 - \tau_2)} \\ &\quad \times \langle \mathcal{T} \tilde{B}_L(t - \tau) \tilde{B}_R^\dagger(t) \tilde{B}_-^\dagger(\tau_1) \tilde{B}_R(\tau_2) \rangle E(\tau_1) E^*(\tau_2). \end{aligned} \quad (11)$$

Depending on the time ordering of various operators, Eq. (11) can be separated into various *Liouville space pathways*. $B_L(t - \tau)$ destroys an exciton at time $t - \tau$ from the left. Thus in order to have a finite signal, we must first create an exciton from the left at an earlier time. $B_L^\dagger(\tau_1)$, which creates the exciton from the left, must therefore act before $B_L(t - \tau)$. That is, we must have $t - \tau > \tau_1$. A similar argument holds for the right operators and $B_R(\tau_2)$, which creates an exciton from right, must act before $B_R^\dagger(t)$, which destroys the exciton. Thus we have $t > \tau_2$. The various time orderings result in the six pathways whose Feynman diagrams are shown in Fig. 1. The three pathways corresponding to $\tau > 0$ and $\tau < 0$ are complex conjugates and the fluorescence signal

$$S(\omega_S, \omega_L, t) = -\frac{2}{\hbar^4} \text{Re} \int_0^\infty d\tau \int_{-\infty}^{t-\tau} d\tau_1 \int_{-\infty}^{\tau_1} d\tau_2 e^{-i\omega_S \tau} e^{-i\omega_L(\tau_1 - \tau_2)} \\ \times \langle \tilde{T} \tilde{B}_L(t-\tau) \tilde{B}_R^\dagger(t) \tilde{B}_L^\dagger(\tau_1) \tilde{B}_R(\tau_2) \rangle E(\tau_1) E^*(\tau_2) \quad (12)$$

can be written as

$$S(\omega_S, \omega_L, t) = -\frac{2}{\hbar^4} \text{Re} [S_I(\omega_S, \omega_L) + S_{II}(\omega_S, \omega_L) + S_{III}(\omega_S, \omega_L)] \quad (13)$$

where the three contributions [Fig. 1(a)] are given by

$$S_I(\omega_S, \omega_L, t) = \int_0^\infty d\tau \int_{-\infty}^{t-\tau} d\tau_1 \int_{-\infty}^{\tau_1} d\tau_2 e^{-i\omega_S \tau} e^{-i\omega_L(\tau_1 - \tau_2)} \\ \times \langle \tilde{B}_R^\dagger(t) \tilde{B}_L(t-\tau) \tilde{B}_L^\dagger(\tau_1) \tilde{B}_R(\tau_2) \rangle E(\tau_1) E^*(\tau_2), \quad (14)$$

$$S_{II}(\omega_S, \omega_L, t) = \int_0^\infty d\tau \int_{-\infty}^{t-\tau} d\tau_2 \int_{-\infty}^{\tau_2} d\tau_1 e^{-i\omega_S \tau} e^{-i\omega_L(\tau_1 - \tau_2)} \\ \times \langle \tilde{B}_R^\dagger(t) \tilde{B}_L(t-\tau) \tilde{B}_R(\tau_2) \tilde{B}_L^\dagger(\tau_1) \rangle E(\tau_1) E^*(\tau_2), \quad (15)$$

$$S_{III}(\omega_S, \omega_L, t) = \int_{-\infty}^t d\tau_2 \int_{t-\tau_2}^\infty d\tau \int_{-\infty}^{t-\tau} d\tau_1 e^{-i\omega_S \tau} e^{-i\omega_L(\tau_1 - \tau_2)} \\ \times \langle \tilde{B}_R^\dagger(t) \tilde{B}_R(\tau_2) \tilde{B}_L(t-\tau) \tilde{B}_L^\dagger(\tau_1) \rangle E(\tau_1) E^*(\tau_2). \quad (16)$$

Changing integration variables and recasting the correlation functions in Hilbert space,

$$\langle \tilde{B}_R^\dagger(t) \tilde{B}_L(t-\tau) \tilde{B}_L^\dagger(t-\tau-\tau_1) \tilde{B}_R(t-\tau-\tau_1-\tau_2) \rangle \\ \equiv \langle \tilde{B}(t-\tau-\tau_1-\tau_2) \tilde{B}^\dagger(t) \tilde{B}(t-\tau) \tilde{B}^\dagger(t-\tau-\tau_1) \rangle, \quad (17)$$

$$\langle \tilde{B}_R^\dagger(t) \tilde{B}_L(t-\tau) \tilde{B}_L^\dagger(t-\tau-\tau_1-\tau_2) \tilde{B}_R(t-\tau-\tau_1) \rangle \\ \equiv \langle \tilde{B}(t-\tau-\tau_1) \tilde{B}^\dagger(t) \tilde{B}(t-\tau) \tilde{B}^\dagger(t-\tau-\tau_1-\tau_2) \rangle, \quad (18)$$

$$\langle \tilde{B}_R^\dagger(t) \tilde{B}_R(t-\tau_2) \tilde{B}_L(t-\tau-\tau_2) \tilde{B}_L^\dagger(t-\tau-\tau_1-\tau_2) \rangle \\ \equiv \langle \tilde{B}(t-\tau_2) \tilde{B}^\dagger(t) \tilde{B}(t-\tau-\tau_2) \tilde{B}^\dagger(t-\tau-\tau_1-\tau_2) \rangle, \quad (19)$$

we obtain

$$S_I(\omega_S, \omega_L, t) = \int_0^\infty d\tau \int_0^\infty d\tau_1 \int_0^\infty d\tau_2 e^{-i\omega_S \tau} e^{-i\omega_L \tau_2} E(t-\tau-\tau_1) \\ \times E^*(t-\tau-\tau_1-\tau_2) \\ \times \langle B(t-\tau-\tau_1-\tau_2) B^\dagger(t) B(t-\tau) B^\dagger(t-\tau-\tau_1) \rangle. \quad (20)$$

$$S_{II}(\omega_S, \omega_L, t) = \int_0^\infty d\tau \int_0^\infty d\tau_1 \int_0^\infty d\tau_2 e^{-i\omega_S \tau} e^{i\omega_L \tau_1} \\ \times E(t-\tau-\tau_1-\tau_2) E^*(t-\tau-\tau_2) \\ \times \langle B(t-\tau-\tau_2) B^\dagger(t) B(t-\tau) B^\dagger(t-\tau-\tau_1-\tau_2) \rangle. \quad (21)$$

$$S_{III}(\omega_S, \omega_L, t) = \int_0^\infty d\tau \int_0^\infty d\tau_1 \int_0^\infty d\tau_2 e^{-i(\omega_S - \omega_L)\tau} e^{-i\omega_S \tau_2} e^{i\omega_L \tau_1} \\ \times E(t-\tau-\tau_1-\tau_2) E^*(t-\tau_2) \\ \times \langle B(t-\tau_2) B^\dagger(t) B(t-\tau-\tau_2) B^\dagger(t-\tau-\tau_1-\tau_2) \rangle. \quad (22)$$

We now insert a complete set of many-body states denoted by $|a\rangle$, $|b\rangle$, $|c\rangle$, and $|d\rangle$, where $|a\rangle$ and $|c\rangle$ are vibronic states belonging to the ground electronic state and $|b\rangle$ and $|d\rangle$ denote the excited states. This gives

$$\langle B(t-\tau-\tau_1-\tau_2) B^\dagger(t) B(t-\tau) B^\dagger(t-\tau-\tau_1) \rangle \\ = \sum_{a,b,c,d} P(a) B_{ab} B_{bc}^\dagger B_{cd} B_{da}^\dagger \\ \times e^{i(\omega_{bc} + i\Gamma_{bc})\tau} e^{i(\omega_{bd} + i\Gamma_{bd})\tau_1} e^{i(\omega_{ba} + i\Gamma_{ba})\tau_2}. \quad (23)$$

Here $P(a)$ is the equilibrium probability of finding the system in state $|a\rangle$, $B_{ab} \equiv \langle a|B|b\rangle$ and $\omega_{ab} \equiv \omega_a - \omega_b$ is the transition frequency between states $|a\rangle$ and $|b\rangle$. $\Gamma_{ab} = (\gamma_a + \gamma_b)/2 + \hat{\Gamma}_{ab}$ is the dephasing rate of the $|a\rangle \rightarrow |b\rangle$ transition.²⁶ Substituting Eq. (23) in Eq. (20), carrying out the time integrals, and assuming stationary field envelopes [$E(t) = 1$], we obtain [Eq. (9.14) of Ref. 26]

$$S_I(\omega_S, \omega_L) = -i \sum_{a,b,c,d} P(a) B_{ab} B_{bc} B_{cd} B_{da} \left(\frac{1}{(\omega_{bc} - \omega_S + i\Gamma_{bc})(\omega_{bd} + i\Gamma_{bd})(\omega_{ba} - \omega_L + i\Gamma_{ba})} \right). \quad (24)$$

Similarly for the other pathways, we get

$$S_{II}(\omega_S, \omega_L) = -i \sum_{a,b,c,d} P(a) B_{ab} B_{bc} B_{cd} B_{da} \left(\frac{1}{(\omega_L - \omega_{da} + i\Gamma_{da})(\omega_{bd} + i\Gamma_{bd})(\omega_{bc} - \omega_S + i\Gamma_{bc})} \right), \quad (25)$$

$$S_{III}(\omega_S, \omega_L) = -i \sum_{a,b,c,d} P(a) B_{ab} B_{bc} B_{cd} B_{da} \left(\frac{1}{(\omega_L - \omega_S - \omega_{ca} + i\Gamma_{ca})(\omega_{bc} - \omega_S + i\Gamma_{bc})(\omega_L - \omega_{da} + i\Gamma_{da})} \right). \quad (26)$$

In the absence of dephasing, $\Gamma_{ab}=0$, substituting Eqs. (24)–(26) in Eq. (13) gives

$$S(\omega_S, \omega_L) = \frac{2\pi}{\hbar^4} \sum_{ac} P(a) \left| \sum_b \frac{B_{cb} B_{ba}}{\omega_L - \omega_{ba} + i\eta} \right|^2 \delta(\omega_L - \omega_S - \omega_{ca}), \quad (27)$$

where η is an infinitesimal positive number. This is the standard expression for spontaneous light emission spectra.²⁶

In the next section, we follow the same steps to compute the fluorescence signal induced by an electric current in a molecular junction.

III. THE CURRENT-INDUCED FLUORESCENCE SPECTRUM

In a STM junction an electron or a hole is injected from the tip to the substrate. To describe this process in an open system, where the number of electrons is not fixed, we can no longer work with exciton variables (B) alone and need to use electron creation and annihilation operators ψ^\dagger and ψ , which satisfy the Fermi anticommutation relations

$$\{\psi_i, \psi_j^\dagger\} = \delta_{ij}, \quad \{\psi_i, \psi_j\} = \{\psi_i^\dagger, \psi_j^\dagger\} = 0. \quad (28)$$

We shall use latin (i, j, k) and greek (μ, η, ν) indices for the substrate and the tip orbitals, respectively.

The total Hamiltonian is given by^{35–37}

$$H_T = H_t + H_s + H_{ts}. \quad (29)$$

It represents the tip (H_t), the substrate (H_s), and their coupling

$$H_{ts} = C^\dagger + C, \quad (30)$$

where

$$C^\dagger = \sum_i \psi_i^\dagger \phi_i, \quad C = \sum_i \phi_i^\dagger \psi_i \quad (31)$$

with $\phi_i = \sum_\mu J_{i\mu} \psi_\mu$, $J_{i\mu}$ are the tunneling matrix elements between the tip and the substrate. In LIF an excitation is created via the interaction with the external electric field whereas in CIF it is created through coupling with the STM tip. The excitation energy is controlled by the applied bias across the STM junction. Thus the bias voltage (V) plays the same role as the frequency ω_L in LIF.

To calculate the fluorescence signal we need the dipole operator $\mu = B + B^\dagger$, where

$$B = \sum_{i < j} \mu_{ij} \psi_i^\dagger \psi_j, \quad (32)$$

$$B^\dagger = \sum_{i < j} \mu_{ji} \psi_j^\dagger \psi_i,$$

and μ_{ij} is the transition dipole between the i th and j th orbitals with energies ϵ_i and ϵ_j , respectively. In the summations in

Eq. (32), we only include terms with $\epsilon_j > \epsilon_i$. Thus B lowers the molecular energy by transferring an electron from a higher orbital j to a lower orbital i while B^\dagger represents the reverse process.

Following the same steps of the previous section, the signal Eq. (8) can be written in the interaction picture [Eq. (4)] where $H = H_t + H_s$. The lowest-order contribution (second order in tip-molecule interaction), in analogy with Eq. (10), gives

$$S(\omega_S, V, t) = -\frac{1}{2\hbar^4} \int d\tau \int d\tau_1 \int d\tau_2 e^{-i\omega_S \tau} \times \langle \mathcal{T} \tilde{B}_L(t - \tau) \tilde{B}_R^\dagger(t) \tilde{H}_{ts}(\tau_1) \tilde{H}_{ts}^\dagger(\tau_2) \rangle. \quad (33)$$

The bias (V) dependence on the right-hand side of Eq. (33) is contained in the density matrix $\rho(t \rightarrow -\infty)$ over which the trace is taken. We shall make the V dependence explicit by factorizing the average in Eq. (33). Expressing H_{ts} in terms of L/R operators [Eq. (5)] and noting that for the signal not to vanish we must have one pair of operators acting from the left and another pair acting from the right, Eq. (33) reduces to

$$S(\omega_S, V, t) = \frac{1}{\hbar^4} \int d\tau \int d\tau_1 \int d\tau_2 e^{-i\omega_S \tau} \times \langle \mathcal{T} \tilde{B}_L(t - \tau) \tilde{B}_R^\dagger(t) \tilde{H}_L^{ts}(\tau_1) \tilde{H}_R^{ts\dagger}(\tau_2) \rangle \quad (34)$$

where $H_\alpha^{ts} = C_\alpha^\dagger + C_\alpha$, $\alpha = L, R$, are superoperators corresponding to Eq. (34), which is analogous to Eq. (11). Using Eq. (30), it can be separated into two terms $S = S_n + S_p$, where

$$S_n(\omega_S, V, t) = \frac{1}{\hbar^4} \int d\tau \int d\tau_1 \int d\tau_2 e^{-i\omega_S \tau} \times \langle \mathcal{T} \tilde{B}_L(t - \tau) \tilde{B}_R^\dagger(t) \tilde{C}_L^\dagger(\tau_1) \tilde{C}_R(\tau_2) \rangle, \quad (35)$$

$$S_p(\omega_S, V, t) = \frac{1}{\hbar^4} \int d\tau \int d\tau_1 \int d\tau_2 e^{-i\omega_S \tau} \times \langle \mathcal{T} \tilde{B}_L(t - \tau) \tilde{B}_R^\dagger(t) \tilde{C}_L(\tau_1) \tilde{C}_R^\dagger(\tau_2) \rangle \quad (36)$$

The operators C_L^\dagger and C_R , Eq. (31), transfer an electron from the tip to the molecule while C_L and C_R^\dagger remove an electron from the molecule. Thus S_n and S_p represent two scenarios for the fluorescence coming from either a nega-

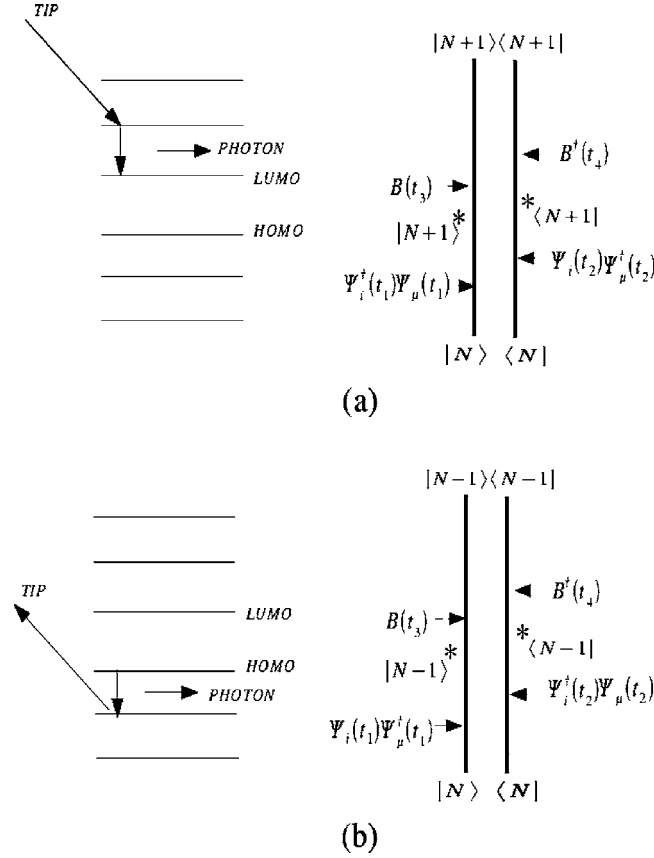


FIG. 2. Double-sided Feynman diagrams for CIF. The molecule is initially in the ground state with N electrons. (a) Emission from a negatively charged molecule (S_n). An electron is transferred from the tip to the molecular orbital (LUMO+1), creating an excited state of the $(N+1)$ -electron system (represented by a star). The system then relaxes to the ground $N+1$ electron state by emitting a phonon. (b) Emission from a positively charged molecule (S_p). An electron is transferred from the molecular orbital HOMO-1 to the tip. This creates an excited state of the $(N-1)$ -electron system. The system relaxes to the ground $N-1$ electron state by transferring an electron from HOMO to HOMO-1 orbital accompanied by a photon emission.

tively or a positively charged molecule, respectively. These contributions are controlled by the polarity of the applied bias.

We first consider S_n . The Feynman diagram for this process is depicted in Fig. 2(a). In Eq. (35), $\langle \dots \rangle$ represents the trace with respect to the initial density matrix of the molecule+tip system at $t \rightarrow -\infty$, which is a product of density matrices of the tip and the molecule alone. The operators B_L and B_R^\dagger bring the injected electron to one of the lower energy orbitals. In order to have a finite signal, C_L^\dagger and C_R must act before B_L and B_R^\dagger . That is, $t - \tau > \tau_1$ and $t > \tau_2$ and we have

$$S_n(\omega_S, V, t) = \frac{1}{\hbar^4} \int d\tau \int_{-\infty}^{t-\tau} d\tau_1 \int_{-\infty}^t d\tau_2 e^{-i\omega_S \tau} \times \langle \mathcal{T} \tilde{B}_L(t-\tau) \tilde{B}_R^\dagger(t) \tilde{C}_L^\dagger(\tau_1) \tilde{C}_R(\tau_2) \rangle. \quad (37)$$

We next express the operators B_L , B_R^\dagger , C_L^\dagger , and C_R in terms of

the field operators [Eqs. (31) and (32)]. Noting that the initial density matrix $\rho(t \rightarrow -\infty)$ is a direct product of ground-state density matrices for the tip and the molecule, the average in Eq. (37) can be factorized into a product of tip and molecule terms,

$$S_n(\omega_S, V, t) = \frac{i}{\hbar^3} \int d\tau \int_{-\infty}^{t-\tau} d\tau_1 \int_{-\infty}^t d\tau_2 e^{-i\omega_S \tau} \times \sum_{i < j} \sum_{i' < j'} \sum_{kl} \sum_{\mu\nu} \mu_{ij} \mu_{i'j'} J_{k\mu} J_{l\nu} \times G_{LR}^{\mu\nu}(\tau_1, \tau_2) \langle \mathcal{T} \tilde{\psi}_{iL}^\dagger(t-\tau) \tilde{\psi}_{jL}(t-\tau) \tilde{\psi}_{j'R}^\dagger(t) \tilde{\psi}_{i'R}(t) \times \tilde{\psi}_{kL}^\dagger(\tau_1) \tilde{\psi}_{lR}(\tau_2) \rangle \quad (38)$$

where

$$G_{LR}^{\mu\nu}(\tau_1, \tau_2) = -\frac{i}{\hbar} \langle \mathcal{T} \tilde{\psi}_{\mu L}(\tau_1) \tilde{\psi}_{\nu R}^\dagger(\tau_2) \rangle_{iip} \quad (39)$$

is the nonequilibrium tip Green's function²⁴ where $\langle \dots \rangle_{iip}$ represents the trace with respect to the tip density matrix. In Hilbert space notation, $G_{LR}^{\mu\nu}$ corresponds to the "lesser" Green's function $G_{\mu\nu}^<$ ^{19,23}

$$G_{LR}^{\mu\nu}(\tau_1, \tau_2) \equiv G_{\mu\nu}^<(\tau_1, \tau_2) = \frac{i}{\hbar} \langle \tilde{\psi}_{\nu}^\dagger(\tau_2) \tilde{\psi}_{\mu}(\tau_1) \rangle_{iip}. \quad (40)$$

Hereafter $\langle \dots \rangle$ will represent the trace with respect to the density matrix of the molecule alone.

We shall model the metal tip as a free electron gas at zero temperature. We then have

$$\sum_{\mu\nu} G_{LR}^{\mu\nu}(\tau_1, \tau_2) = \frac{i}{\hbar} \sum_{\mu}^{occ} e^{-i(\hbar\epsilon)\epsilon_\mu(\tau_1-\tau_2)} \quad (41)$$

where ϵ_μ is the energy of the μ th orbital and sum runs over the all occupied states. Assuming that the tip energy bands constitute a continuum, we write

$$\sum_{\mu\nu} G_{LR}^{\mu\nu}(\tau_1, \tau_2) = \frac{i}{\hbar} \int_{-\infty}^{E_F+eV} d\epsilon \varrho(\epsilon) e^{-i(\hbar\epsilon)\epsilon(\tau_1-\tau_2)} \quad (42)$$

where E_F is the Fermi energy of the metal and V is the applied bias. E_F+eV is the highest filled energy and $\varrho(\epsilon)$ is the tip density of states.

Substituting Eq. (42) in Eq. (38), we obtain

$$S_n(\omega_S, V, t) = \frac{1}{\hbar^4} \int d\tau \int_{-\infty}^{t-\tau} d\tau_1 \int_{-\infty}^t d\tau_2 \int_{-\infty}^{E_F+eV} d\epsilon \times \sum_{i < j} \sum_{i' < j'} \sum_{kl} \mu_{ij} \mu_{i'j'} J_k(\epsilon) J_l(\epsilon) \varrho(\epsilon) e^{-i\omega_S \tau} e^{-i(\hbar\epsilon)\epsilon(\tau_1-\tau_2)} \times \langle \mathcal{T} \tilde{\psi}_{iL}^\dagger(t-\tau) \tilde{\psi}_{jL}(t-\tau) \tilde{\psi}_{j'R}^\dagger(t) \tilde{\psi}_{i'R}(t) \tilde{\psi}_{kL}^\dagger(\tau_1) \tilde{\psi}_{lR}(\tau_2) \rangle \quad (43)$$

where $J_k(\epsilon)$ is the coupling between the k th orbital of the molecule and the energy continuum of the tip. In analogy to

LIF [Eq. (11)], depending on the time ordering of various operators, \mathcal{S}_n contains contributions from six LSPs. The Feynman diagrams for these LSPs can be obtained from Fig. 1 by replacing the first two B operators acting at times τ_1 and τ_2 with Fermi operators ψ_k^\dagger and ψ_l , respectively. The total

signal $\mathcal{S}_n = (\mathcal{S}_n^I + \mathcal{S}_n^{II} + \mathcal{S}_n^{III}) + \text{c.c.}$, where \mathcal{S}_n^I , \mathcal{S}_n^{II} , and \mathcal{S}_n^{III} are computed in Appendix B. For a more direct correspondence with LIF, we shall consider the derivative of the signal with respect to the applied bias (V). This gives in Hilbert space (Appendix B),

$$\begin{aligned} \frac{d\mathcal{S}_n^I(\omega_S, V, t)}{dV} &= \frac{e}{\hbar^4} \int_0^\infty dt_1 \int_0^\infty dt_2 \int_0^\infty dt_3 \sum_{i < j} \sum_{i' < j'} \sum_{kl} \mu_{ij} \mu_{i'j'} J_k(E_F + eV) J_l(E_F + eV) e^{-i\omega_S t_1} \varrho(E_F + eV) e^{-(i/\hbar)(E_F + eV)t_3} \\ &\quad \times \langle \tilde{\psi}_l(t - t_1 - t_2 - t_3) \tilde{\psi}_{j'}^\dagger(t) \tilde{\psi}_{i'}(t) \tilde{\psi}_i^\dagger(t - t_1) \tilde{\psi}_j(t - t_1) \tilde{\psi}_k^\dagger(t - t_1 - t_2) \rangle, \end{aligned} \quad (44)$$

$$\begin{aligned} \frac{d\mathcal{S}_n^{II}(\omega_S, V, t)}{dV} &= \frac{e}{\hbar^4} \int_0^\infty dt_1 \int_0^\infty dt_2 \int_0^\infty dt_3 \sum_{i < j} \sum_{i' < j'} \sum_{kl} \mu_{ij} \mu_{i'j'} J_k(E_F + eV) J_l(E_F + eV) e^{-i\omega_S t_1} \varrho(E_F + eV) e^{(i/\hbar)(E_F + eV)t_3} \\ &\quad \times \langle \tilde{\psi}_l(t - t_1 - t_2) \tilde{\psi}_{j'}^\dagger(t) \tilde{\psi}_{i'}(t) \tilde{\psi}_i^\dagger(t - t_1) \tilde{\psi}_j(t - t_1) \tilde{\psi}_k^\dagger(t - t_1 - t_2 - t_3) \rangle, \end{aligned} \quad (45)$$

$$\begin{aligned} \frac{d\mathcal{S}_n^{III}(\omega_S, V, t)}{dV} &= \frac{e}{\hbar^4} \int_0^\infty dt_1 \int_0^\infty dt_2 \int_0^\infty dt_3 \sum_{i < j} \sum_{i' < j'} \sum_{kl} \mu_{ij} \mu_{i'j'} J_k(E_F + eV) J_l(E_F + eV) \varrho(E_F + eV) e^{-i\omega_S(t_1 + t_3)} e^{-(i/\hbar)(E_F + eV)(t_2 + t_3)} \\ &\quad \times \langle \tilde{\psi}_l(t - t_3) \tilde{\psi}_{j'}^\dagger(t) \tilde{\psi}_{i'}(t) \tilde{\psi}_i^\dagger(t - t_1 - t_2) \tilde{\psi}_j(t - t_1 - t_2) \tilde{\psi}_k^\dagger(t - t_1 - t_2 - t_3) \rangle. \end{aligned} \quad (46)$$

Equations (44)–(46) are analogous to Eqs. (20)–(22). Expanding them in many-body molecular states $|a\rangle$, $|b\rangle$, $|c\rangle$, and $|d\rangle$ and neglecting dephasing gives (see Appendix C),

$$\frac{d\mathcal{S}_n(\omega_S, V)}{dV} = \frac{2\pi e}{\hbar} \sum_{ac} P(a) \left| \sum_{i < j} \sum_k \sum_b \frac{\mu_{ij} \langle a | \psi_k | b \rangle \langle b | \psi_j^\dagger \psi_i | c \rangle J_k(E_F + eV)}{E_F + eV - \hbar\omega_{ba} + i\eta} \right|^2 \varrho(E_F + eV) \delta(E_F + eV - \hbar\omega_S + \hbar\omega_{ca}). \quad (47)$$

Unlike LIF, the many-body states $|a\rangle$, $|b\rangle$, and $|c\rangle$ in Eq. (47) correspond to a molecule with different numbers of electrons. $|a\rangle$ is the ground state $|N\rangle$ with N electrons. $|b\rangle$ represents the excited state $|N+1\rangle^{(**)}$ with $N+1$ electrons, and $|c\rangle$ represents some lower lying excited state $|N+1\rangle^{(*)}$ of $N+1$ electrons. $J_k(E_F + eV)$ is the coupling of the k th molecular orbital with the highest-energy band of the tip. Since molecular orbitals have different spatial profiles, $J_k(E_F + eV)$, which depends on the overlap of the molecular orbitals with the tip states, and the fluorescence spectrum will vary as the tip is scanned across the molecule.

In summary when the tip is negatively biased with respect to the molecule, an electron is injected into one of the unoccupied orbitals of the molecule. This electron then makes a radiative transition to one of the lower orbitals, emitting a photon, before moving to the metal surface. In order to observe CIF, the electron from the tip must be transferred to any orbital higher than the lowest unoccupied molecular orbital (LUMO), so that the negative ion is created in an electronically excited state.

Following the same steps that lead from Eq. (35) to Eq. (38), the signal \mathcal{S}_p [Eq. (36)] from a positively charged molecule can be expressed as

$$\begin{aligned} \mathcal{S}_p(\omega_S, V, t) &= \frac{i}{\hbar^3} \int d\tau \int_{-\infty}^{t-\tau} d\tau_1 \int_{-\infty}^{\tau} d\tau_2 e^{-i\omega_S \tau} \\ &\quad \times \sum_{i < j} \sum_{i' < j'} \sum_{kl} \sum_{\mu\nu} \mu_{ij} \mu_{i'j'} J_{k\mu} J_{l\nu} G_{RL}^{\nu\mu}(\tau_2, \tau_1) \\ &\quad \times \langle \mathcal{T} \tilde{\psi}_{iL}^\dagger(t - \tau) \tilde{\psi}_{jL}(t - \tau) \tilde{\psi}_{j'R}^\dagger(t) \tilde{\psi}_{i'R}(t) \tilde{\psi}_{kL}(\tau_1) \tilde{\psi}_{lR}^\dagger(\tau_2) \rangle \end{aligned} \quad (48)$$

with the Green's function²⁴

$$G_{RL}^{\nu\mu}(\tau_2, \tau_1) = -\frac{i}{\hbar} \langle \mathcal{T} \tilde{\psi}_{\nu R}(\tau_2) \tilde{\psi}_{\mu L}^\dagger(\tau_1) \rangle_t. \quad (49)$$

This process is shown in Fig. 2(b). In Hilbert space, $G_{RL}^{\nu\mu}$ corresponds to the “greater” Green's function $G_{\nu\mu}^>$ ^{19,21}

$$G_{RL}^{\nu\mu}(\tau_1, \tau_2) \equiv -G_{\nu\mu}^>(\tau_1, \tau_2) = \frac{i}{\hbar} \langle \tilde{\psi}_\nu(\tau_2) \tilde{\psi}_\mu^\dagger(\tau_1) \rangle. \quad (50)$$

Assuming the tip to be a free electron gas, we can write

$$\sum_{\mu\nu} G_{RL}^{\nu\mu}(\tau_2, \tau_1) = \frac{i}{\hbar} \sum_{\mu}^{\text{unocc}} e^{-(i/\hbar)\epsilon_{\mu}(\tau_2 - \tau_1)} \quad (51)$$

where μ runs over all unoccupied orbitals. Substituting this in Eq. (48) and assuming that the tip energy states form a continuum, we get

$$\begin{aligned} \mathcal{S}_p(\omega_S, V, t) &= \frac{-1}{\hbar^4} \sum_{i < j} \sum_{i' < j'} \sum_{kl} \mu_{ij} \mu_{i'j'} \int d\tau \int_{-\infty}^{t-\tau} d\tau_1 \int_{-\infty}^t d\tau_2 \\ &\times \int_{E_F + eV}^{\infty} d\epsilon J_k(\epsilon) J_l(\epsilon) \varrho(\epsilon) e^{-i\omega_S \tau} e^{-(i/\hbar)\epsilon(\tau_2 - \tau_1)} \\ &\times \langle T \tilde{\psi}_{iL}^{\dagger}(t - \tau) \tilde{\psi}_{jL}(t - \tau) \tilde{\psi}_{j'R}^{\dagger}(t) \tilde{\psi}_{i'R}(t) \tilde{\psi}_{kL}(\tau_1) \tilde{\psi}_{lR}^{\dagger}(\tau_2) \rangle. \end{aligned} \quad (52)$$

Proceeding along the steps that led from Eq. (43) to Eq. (47), the rate of change of \mathcal{S}_p with respect to applied bias is obtained as

$$\begin{aligned} \frac{d\mathcal{S}_p(\omega_S, V)}{dV} &= \frac{2\pi e}{\hbar} \sum_{ac} P(a) \\ &\times \left| \sum_{i < j} \sum_{k,b} \frac{\langle a | \psi_i^{\dagger} | b \rangle \langle b | \psi_j^{\dagger} \psi_i | c \rangle \mu_{ij} J_k(E_F + eV)}{E_F + eV - \hbar\omega_{ab} + i\eta} \right|^2 \\ &\times \varrho(E_F + eV) \delta(E_F + eV + \hbar\omega_S + \hbar\omega_{ca}) \end{aligned} \quad (53)$$

where $|a\rangle$ denotes the ground state of N electrons, $|b\rangle$ and $|d\rangle$

are excited states $|N-1\rangle^{(**)}$ of a molecule with $N-1$ electrons, and $|c\rangle$ is a lower excited state $|N-1\rangle^{(*)}$ with $N-1$ electrons.

In \mathcal{S}_p , an electron is transferred from one of the occupied orbitals lying below the highest occupied molecular orbital (HOMO) of the molecule to the tip. This creates a positive ion in an electronically excited state. To observe CIF, an electron from one of the orbitals makes a transition to the orbital from which electron is transferred. \mathcal{S}_n involves initially unoccupied orbitals and takes place in the negatively charged molecule whereas \mathcal{S}_p involves initially occupied levels and takes place in the positively charged substrate. Electroluminescence³ involves the simultaneous injection of both an electron and a hole into the molecule, and the light is emitted from the neutral molecule. This is a higher-order process (fourth order in H_{ts}) that goes beyond the present theory.

IV. GREEN'S FUNCTION EXPRESSIONS FOR THE FLUORESCENCE SPECTRUM

At the density-functional (or Hartree Fock) level,³⁸ the electronic states are given by a single Slater determinant and the fluorescence signals Eqs. (35) and (36) can be expanded in terms of the orbital energies. The time evolution of operators in the interaction picture is

$$\tilde{\psi}_i(t) = e^{iHt} \psi_i e^{-iHt} = e^{-i\epsilon_i t} \psi_i, \quad (54)$$

where H is the molecular Hamiltonian and ϵ_i is the energy of the i th orbital. In this case Eq. (43) gives (see Appendix D)

$$\frac{d\mathcal{S}_n(\omega_S, V)}{dV} = \frac{2e}{\hbar} \text{Im} \sum_{i < j, j'}^{\text{unocc}} \sum_{jj'}^{\text{unocc}} \frac{\mu_{ij} \mu_{i'j'} J_j(E_F + eV) J_{j'}(E_F + eV) \varrho(E_F + eV)}{(E_F + eV - \epsilon_j + i\Gamma_{Vj})(\epsilon_{j'} - E_F + eV + i\Gamma_{j'V})(E_F + eV - \epsilon_i - \hbar\omega_S + i\Gamma_{iV})}, \quad (55)$$

where Γ_{Vj} is the dephasing rate of the coherence between the j th molecular orbital and tip state with energy $E_F + eV$. Similarly, for \mathcal{S}_p we obtain

$$\frac{d\mathcal{S}_p(\omega_S, V)}{dV} = \frac{2e}{\hbar} \text{Im} \sum_{ii' < j}^{\text{occ}} \sum_j^{\text{occ}} \frac{\mu_{ij} \mu_{i'j} J_i(E_F + eV) J_{i'}(E_F + eV) \varrho(E_F + eV)}{(\epsilon_i - E_F - eV + i\Gamma_{Vi})(E_F + eV - \epsilon_{i'} + i\Gamma_{i'V})(\epsilon_j - E_F - eV - \hbar\omega_S + i\Gamma_{Vj})}. \quad (56)$$

Note that the sums in $\mathcal{S}_n(\mathcal{S}_p)$ only run over unoccupied (occupied) orbitals.

It is interesting to note that Eqs. (55) and (56) cannot be recast as the modulus square of a complex amplitude, as was the case with the expressions derived using the many-electron states [Eqs. (47)]. This is related to the distinction between Raman and fluorescence processes.²⁶ When summing over many-body states and in the absence of a bath (e.g., phonons), we can think of electron tunneling + photon emission as a single coherent event (like Raman emission in

LIF) which can be described by an amplitude. A single-electron picture in terms of orbitals is a *reduced description* where the many-body states act as a bath of quasiparticles. This bath, as well as other phonon baths, causes the process to be sequential (incoherent). This can no longer be described by an amplitude, as in fluorescence in LIF.²⁶

Using Wick's theorem for Fermi superoperators,²⁵ the CIF signals Eqs. (35) and (36) can be expressed in terms of the nonequilibrium superoperator Green's functions for the non-interacting tip and molecule (Appendix E)

$$\begin{aligned}
\frac{dS_n(\omega_S, V)}{dV} = & ie\hbar^2 \sum_{i < j} \sum_{i' < j'} \sum_{kl} \varrho(E_F + eV) J_k(E_F + eV) J_l(E_F + eV) \mu_{ij} \mu_{i'j'} \int \frac{d\omega}{2\pi} \int \frac{d\omega'}{2\pi} \left(\frac{G_{ji}^{0T}(\omega) G_{i'j'}^{0\bar{T}}(\omega') G_{lk}^{0>}(E_F + eV - \hbar\omega_S)}{\hbar\omega_S^2 + \eta^2} \right. \\
& - \frac{G_{ji}^{0T}(\omega) G_{i'j'}^{0\bar{T}}(\omega') G_{i'k}^{0>}(E_F + eV - \hbar\omega_S)}{(\hbar\omega_S + i\eta)(\omega' + E_F + eV - i\eta)} - \frac{G_{i'i}^{0>}(\omega) G_{jj'}^{0<}(\omega') G_{lk}^{0>}(\omega' - \omega - \hbar\omega_S - E_F - eV)}{(\hbar\omega_S + \omega - \omega')^2 + \eta^2} \\
& + \frac{G_{jk}^{0T}(\omega) G_{i'j'}^{0\bar{T}}(\omega') G_{i'j}^{0>}(E_F + eV - \hbar\omega_S)}{(E_F + eV - \omega' + i\eta)(E_F + eV - \omega - i\eta)} + \frac{G_{li}^{0>}(\omega) G_{i'k}^{0>}(\omega') G_{jj'}^{0<}(\omega + \omega' + \hbar\omega_S - E_F - eV)}{(E_F + eV - \omega' + i\eta)(E_F + eV - \omega - i\eta)} \\
& \left. - \frac{G_{jk}^{0T}(\omega) G_{i'j'}^{0\bar{T}}(\omega') G_{li}^{0>}(E_F + eV - \hbar\omega_S)}{(E_F + eV - \omega + i\eta)(\hbar\omega_S - i\eta)} \right). \tag{57}
\end{aligned}$$

Similarly for S_p , we obtain

$$\begin{aligned}
\frac{dS_p(\omega_S, V)}{dV} = & -ie\hbar^2 \sum_{i < j} \sum_{i' < j'} \sum_{kl} \varrho(E_F + eV) J_k(E_F + eV) J_l(E_F + eV) \mu_{ij} \mu_{i'j'} \int \frac{d\omega}{2\pi} \int \frac{d\omega'}{2\pi} \\
& \times \left(\frac{G_{i'i}^{0>}(\omega) G_{jj'}^{0<}(\omega') G_{kl}^{0<}(\omega - \omega' + \hbar\omega_S + E_F + eV)}{(\omega' - \omega - \hbar\omega_S)^2 + \eta^2} + \frac{G_{i'i}^{0>}(\omega) G_{jl}^{0<}(\omega') G_{kj'}^{0<}(\omega - \omega' + \hbar\omega_S + E_F + eV)}{\hbar(\omega' - \omega - \hbar\omega_S + i\eta)(E_F + eV - \omega' + i\eta)} \right. \\
& - \frac{G_{ji}^{0T}(\omega) G_{i'j'}^{0\bar{T}}(\omega') G_{kl}^{0<}(\hbar\omega_S + E_F + eV)}{\hbar^2\omega_S^2 + \eta^2} - \frac{G_{ji}^{0T}(\omega) G_{i'l}^{0\bar{T}}(\omega') G_{kj'}^{0<}(E_F + eV + \hbar\omega_S)}{(\hbar\omega_S + i\eta)(E_F + eV - \omega' + i\eta)} \\
& \left. + \frac{G_{ki}^{0T}(\omega) G_{i'l}^{0\bar{T}}(\omega') G_{jj'}^{0<}(E_F + eV + \hbar\omega_S)}{(E_F + eV + \omega + i\eta)(E_F + eV - \omega' + i\eta)} + \frac{G_{ki}^{0T}(\omega) G_{jl}^{0<}(E_F + eV + \hbar\omega_S) G_{i'j'}^{0\bar{T}}(\omega')}{(E_F + eV - \omega - i\eta)(\hbar\omega_S + i\eta)} \right). \tag{58}
\end{aligned}$$

$S_n(S_p)$ involves the tip Green's function $G^<(G^>)$ [Eqs. (E3) and (E4)], which corresponds to the occupied (unoccupied) density of states of the tip.^{18,22} In order for S_n to be finite, an electron has to move from one of the occupied tip states to a molecular orbital. This is guaranteed by the tip Green's function $G^<$ in Eq. (E6). Similarly, $G_{\nu\mu}^>$ in Eq. (E7) makes sure that electrons are transferred from the molecule to one of the unoccupied states of the tip.

All many-body interactions (electron-electron, electron-phonon, etc.) in the CIF signals S_n and S_p are formally included in Eqs. (38) and (48). However, computing the necessary six-point (three-particle) Green's functions for a many-body system is a difficult task. They can be computed approximately by replacing all the zeroth-order Green's functions in Eqs. (E6) and (E7) [or Eqs. (57) and (58)] with the full Green's functions (i.e., traced with respect to the density matrix of the interacting system). Invoking this approximation amounts to replacing all the zeroth-order Green's functions G^{0T} , etc., in Eqs. (E6) and (E7) with full Green's functions G^T , etc. The same resummation is usually done in equilibrium calculations of the density-density correlation functions by splitting the average of four operators into the product of two Green's functions, ignoring the vertex corrections.^{39,40} Although this approximation completely ignores the interaction between excitons, it works reasonably well for many systems.⁴⁰ The four Green's functions G^T , $G^{\bar{T}}$,

$G^<$, and $G^>$ can be obtained from the solution of a coupled Keldysh Dyson equation^{18,19,41}

$$\begin{aligned}
\begin{pmatrix} G^T & G^< \\ G^> & G^{\bar{T}} \end{pmatrix} = & \begin{pmatrix} G^{0T} & G^{0<} \\ G^{0>} & G^{0\bar{T}} \end{pmatrix} \\
& + \begin{pmatrix} G^{0T} & G^{0<} \\ G^{0>} & G^{0\bar{T}} \end{pmatrix} \begin{pmatrix} \Sigma^T & \Sigma^< \\ \Sigma^> & \Sigma^{\bar{T}} \end{pmatrix} \begin{pmatrix} G^T & G^< \\ G^> & G^{\bar{T}} \end{pmatrix}, \tag{59}
\end{aligned}$$

where the self-energies Σ include the effect of all many-body interactions and can be expressed in terms of the Green's functions themselves.^{24,37,42} The Green's functions are then computed by solving Eq. (59) self-consistently together with the self-energies. The Green's function expressions provide a way to incorporate the effect of many-body interactions to the fluorescence signal through self-energies and are particularly useful when the interacting bath of electrons and phonons is under nonequilibrium conditions. In that case a perturbative treatment of many-body interactions does not capture the nonequilibrium effects and one needs to solve the Dyson equation self-consistently.

V. COMPUTATIONAL RESULTS

In this section we present computational results for current-induced fluorescence in benzene. Specifically, we ex-

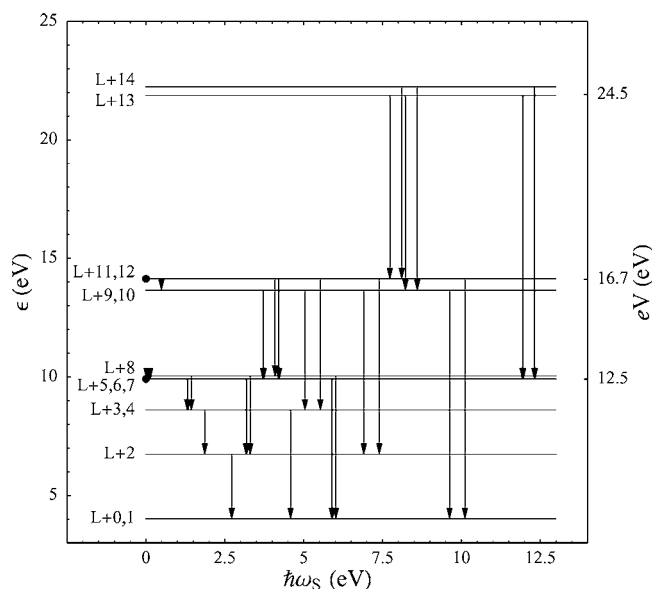


FIG. 3. Energy level scheme for several unoccupied molecular orbitals of neutral benzene. The states are labeled relative to the LUMO (L). The Fermi energy $E_F=2.6$ eV is taken to be the midpoint between the HOMO and LUMO energy levels. Arrows depict the transitions which contribute strongly to the current-induced fluorescence involving the negative anion at positive bias voltage. The left ordinate axis depicts the orbital energies ϵ_i while the right axis indicates the applied bias energy required to induce a transition from a given orbital, $eV=-E_F+\epsilon_i$. The spatial variation of the emission originating from these transitions is examined in Figs. 7–9.

amine the derivative of the fluorescence signal with respect to voltage originating from transitions between the unoccupied molecular orbitals of the benzene anion which occur at positive applied bias; cf. Eq. (55). The unoccupied molecular orbital energies ϵ_i and dipole moment integrals μ_{ij} determine the spectral positions and relative intensities of the peaks in the emission spectrum. These quantities are calculated at the density functional theory (DFT) level with the B3LYP exchange-correlation functional and a modest 3-21G basis set as implemented in the GAUSSIAN 03 package.⁴⁴

Peaks in the fluorescence are expected for transitions between unoccupied orbitals $j \rightarrow i (j > i)$ at photon energies $\hbar\omega_S = \epsilon_j - \epsilon_i$ when the applied bias energy exceeds a threshold determined by energy difference $-E_F + \epsilon_j$. We fixed the Fermi energy of the system $E_F = -2.6$ eV at the midpoint between the HOMO and LUMO. The dephasing rates Γ_{Vi} give a finite width to the molecular orbital energies and determine the line shape of the electronic transitions. These rates have contributions coming from both the substrate and also the coupling to the tip. We treat these as energy-independent parameters with a constant value $\Gamma_{Vi} = 0.8$ eV for all molecular orbitals i . Figure 3 shows the energy level diagram for the 15 lowest unoccupied orbitals. The orbitals are represented as horizontal lines, labeled relative to the LUMO, with the left ordinate axis corresponding to the respective eigenenergies. The dipole-allowed transitions are depicted as vertical arrows where the abscissa axis corresponds to the energy of the emitted photons. The right ordinate axis corresponds to the bias energy threshold at which a given unoccupied molecular orbital opens up to tunneling.

The spatial dependence of the emission signal is determined by the spatial variation of the coupling elements $J_i(E_F + eV)$ between the molecule orbitals and the STM tip as the position of tip is scanned across the molecule. In the Tersoff-Hamann approach to STM,⁴⁵ the wave function at the apex of the tip is represented by an s -wave $|\mathbf{r}_0\rangle$ centered about the position \mathbf{r}_0 . Since the tip has only a single orbital with energy $E_F + eV$, the tip density of states $\rho(\epsilon)$ is unity at $\epsilon = E_F + eV$ and zero for all other energies. The coupling between this tip orbital and a molecular orbital $|\psi_i\rangle$ can be approximated by the overlap integral

$$J_i(E_F + eV) \propto \langle \psi_i | \mathbf{r}_0 \rangle. \quad (60)$$

STM images are related to the local density of states

$$\rho_{\text{LDOS}}(E, \mathbf{r}_0) \propto \sum_i |J_i(E)|^2 \delta(E - \epsilon_i) \quad (61)$$

at energy $E = E_F + eV$. The overlap couplings are computed by introducing an extra s -type basis function centered at the desired tip position and evaluating the atomic overlap integrals with the other basis functions used in the DFT calculation. We include a $51 \times 51 \times 1$ grid of ghost atomic centers positioned 1 \AA above and parallel to the molecular plane of the benzene molecule. Each ghost atom is given a single $1s$ orbital using parameters taken from the 3-21G basis set for silver atoms. The atomic orbital overlaps between the ghost basis functions and real atomic orbitals are combined with the molecular orbital coefficients to compute the J_i couplings. In Fig. 4 we examine the spatial dependence of the coupling elements for the 15 LUMOs identified in Fig. 3. Each panel illustrates the x and y dependence of the $|J_i|^2$ coupling at a distance of $z = 1 \text{ \AA}$ above the molecular plane. The orbitals are labeled relative to the LUMO; the bias threshold energies at which tunneling electrons may populate these orbitals are also given. The LUMO+9 through LUMO+14 are quite extended and therefore have the largest overlap with the tip orbital. We will use these plots of the individual orbitals to better understand the spatial dependence of the emission signal which may involve contributions from multiple unoccupied orbitals.

Figure 5 shows the dS_n/dV signal calculated using Eq. (55) as a function photon energy and bias potential with the tip centered at different positions above benzene molecule, see points labeled 1–9 in Fig. 7(a). The different spectra contain peaks with similar structure but the relative intensities of the peaks clearly depend on the tip's position. The signals at positions 1, 3, 4, and 9 have been scaled by five times to show the underlying spectral features which are suppressed due to the smaller tip-molecule overlap in these regions of space. In Figs. 6(a) and 6(b) we analyze more closely the bias dependence of the peaks enclosed between the dashed lines at positions 5 and 7, respectively. Both cases show that the spectral positions of peak maxima are blue-shifted as the applied bias is increased. Also, the intensities of the dS_n/dV peaks first increase and then decrease as the voltage is scanned over the threshold bias energy for the corresponding transitions. We expect the peak intensity of S_n should saturate to a value determined by the overlap coupling strength and transition dipole moment. However, as the

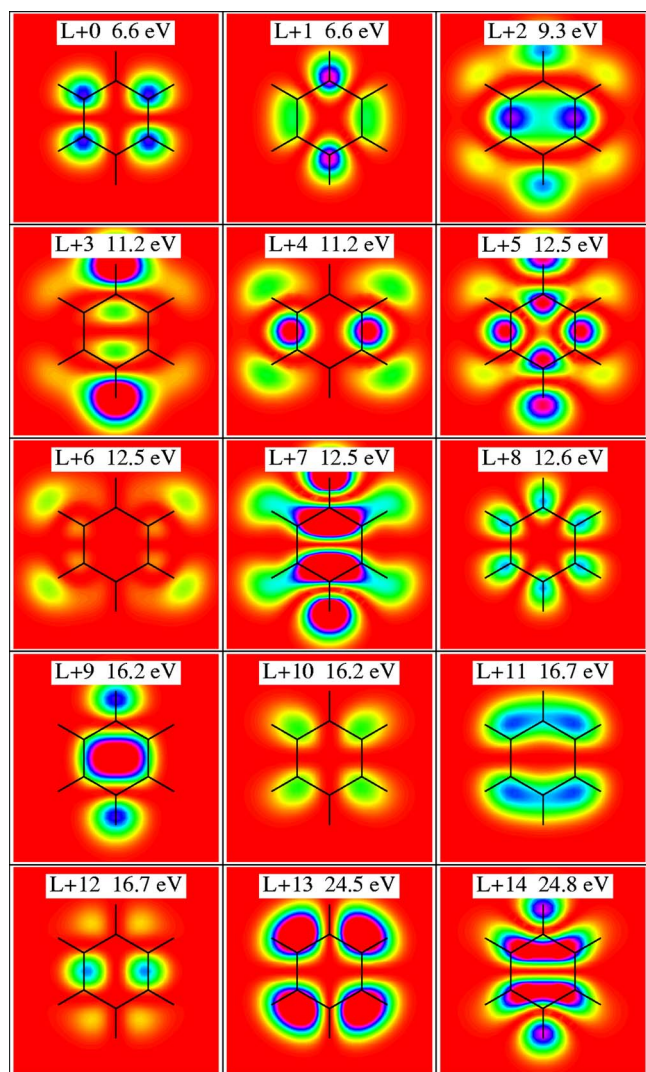


FIG. 4. (Color online) Contour plots of the overlap coupling $J_i(\epsilon_F + eV)^2$ between 15 LUMOs and the tip orbital positioned at a height of 1\AA above the molecular plane. The molecular structure of benzene is superimposed over the images as a visual reference. The threshold bias energy at which these orbitals will accept tunneling electrons are also given. The coupling strength ranges from (red) 0 to (magenta) 1.5×10^{-5} . LUMO+9 through LUMO+14 have the strongest coupling orbitals and are scaled by 10^{-1} .

bias energy increases more tunneling channels will open up, so that state to state transitions between higher lying unoccupied energy levels will also contribute to the S_n . For larger molecules with a more congested electronic spectrum dS_n/dV should be a more useful quantity than S_n since nearly degenerate transitions can be more easily distinguished if they have distinct threshold bias energies. Note also that dS_n/dV is the more direct analog of LIF.

We next turn to the spatial dependence of the fluorescence peaks. Figure 7(a) shows a contour plot of the local density of states at 12.5 eV and sliced 1\AA above the molecular plane. The structure is superimposed on the image as a visual reference. The LUMO+5 through LUMO+8 orbitals strongly contribute to the local density at this bias energy. Shown in panel (b) are the dS_n/dV signals (at constant bias) for the tip

positions corresponding to the white numbers in panel (a). The dashed lines labeled (c)–(f) indicate the photon energies at which significant peaks are found. Again, it is clear that for certain tip positions, different peaks are suppressed or enhanced depending on the overlap coupling. The zero-energy peak (c) stems from transitions between degenerate and near-degenerate orbitals and has large intensity at positions 5, 7, and 8. The spatially resolved peak is shown in Fig. 7(c) and comparison with the overlap couplings in Fig. 4 indicates that the LUMO+7 is the dominant orbital contributing to the spatial structure of this peak with emission to the LUMO+5,6 degenerate orbital pair. Similarly, the spatial dependence of the peak at (d) 1.1 eV resembles both the LUMO+5 and LUMO+7; however, since the transition from LUMO+5 to LUMO+3,4 is dipole forbidden this peak is attributed to the LUMO+7 to LUMO+3,4 transition. The peak at (e) 3.0 eV has several contributions but is dominated by the transition from the LUMO+5 to the LUMO+2. The map of the peak at (f) 5.8 eV appears nearly identical to LUMO+8 and corresponds to emission to the ground state (LUMO+0,1) of the benzene anion.

We can apply this same analysis to the fluorescence peaks predicted at higher bias voltage energies. Figure 8(a) shows the local density of states at 16.7 eV and has strong contributions from LUMO+9,10 and LUMO+11,12 degenerate pairs. The spatially resolved emission spectra, shown in panel (b), are markedly different compared to those shown in Fig. 7(b). The spatially resolved peaks in panels (c), (d), and (f) share common features and appear to be a combination of the LUMO+11,12 degenerate orbitals. They also have similar relative intensities at positions 2, 4-6, and 8. We attribute the low-energy peak at (c) 0.6 eV to transitions from the LUMO+11 to the LUMO+9,10 (note that similar transitions from the LUMO+12 are dipole forbidden). The peak at (d) 4.3 eV involves transitions from LUMO+11,12 to LUMO+5,6 through LUMO+8 orbitals and the higher-energy peak (f) 7.5 eV to emission to the LUMO+2 orbital. Panel (e) is somewhat different from the other three maps and has additional contributions coming from the LUMO+9,10 orbitals and involves emission at 5.6 eV to the LUMO+3,4 orbitals. Figure 9 is similar to Figs. 7 and 8 except that the bias energy is tuned up to 24.5 eV and we see only two major peaks. The peak (c) 7.4 eV corresponds to transitions from LUMO+13 to LUMO+9 and LUMO+11 but not to LUMO+10 and LUMO+12, which are dipole forbidden. The peak at (d) 11.5 eV corresponds to emission from the LUMO+14 to LUMO+5.

VI. DISCUSSION

We have developed a many-body theory of single-molecule fluorescence in STM junctions. The Liouville space superoperator formulation makes it possible to interpret and distinguish between various physical processes that contribute to the signal in real time using double sided Feynman diagrams, and offers a convenient bookkeeping device for the various possible time orderings of interactions. Equations (38) and (48) express the fluorescence signal from negatively and positively charged molecules in terms of the nonequilib-

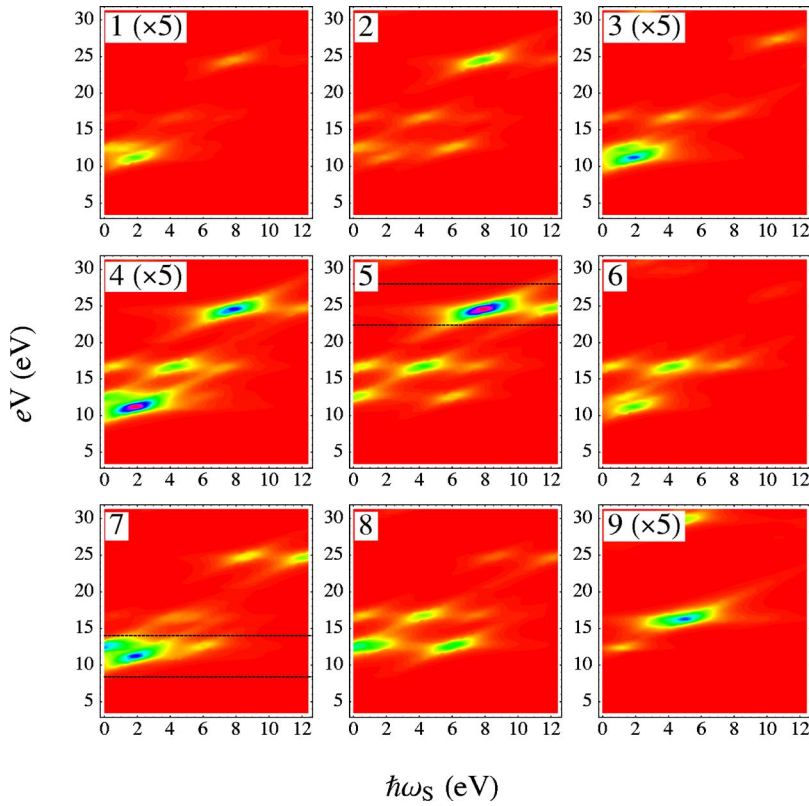


FIG. 5. (Color online) Panels (1)–(9) show the two-dimensional current-induced fluorescence spectrum of benzene as a function of photon energy $\hbar\omega_s$, and bias energy eV at different lateral tip positions [cf. Fig. 7(a)], at constant height 1\AA above the molecule. The intensities are normalized so that from red to magenta is on the order of unity. The weaker spectra for positions (3), (4), and (9) have been scaled by five times.

rium Green's functions of the tip. The expansions in many-body states, Eqs. (47) and (48), include all many-body interactions and are exact. Ignoring many-body interactions (electron-electron, electron-phonon, etc.) in the molecule and using Wick's theorem,²⁵ the three-point correlation functions [Eqs. (38) and (48)] can be alternatively expressed in terms of nonequilibrium Green's functions of the molecule, Eqs. (E6) and (E7).

The signal dependence on tip position comes through the tunneling coefficients $J_k(E)$ which couple the k th orbital of

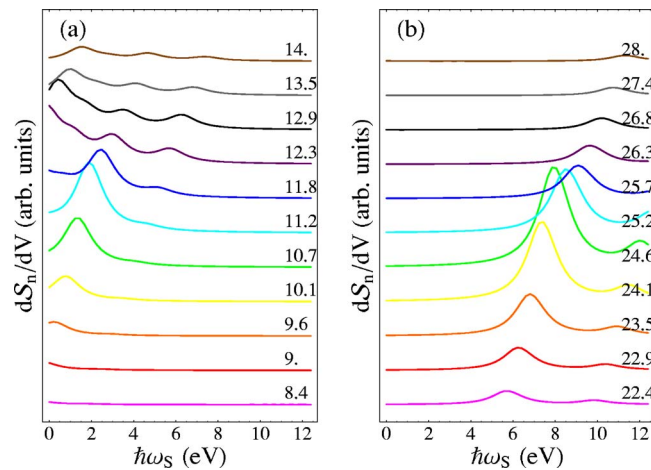


FIG. 6. (Color online) (a) and (b) show two families of one-dimensional spectra calculated at different bias energies between the dashed lines of panels (5) and (7) of Fig. 5, respectively. The spectra demonstrate a blueshift in the peak maximum as the bias voltage increases and are offset vertically for visual clarity.

the molecule with the energy band of the tip at energy E . These elements are proportional to the overlap of the tip and molecular orbitals. Their variations as the tip is scanned across the molecule, controls the fluorescence signal. For zero bias ($V=0$), the signal should vanish. This can be most

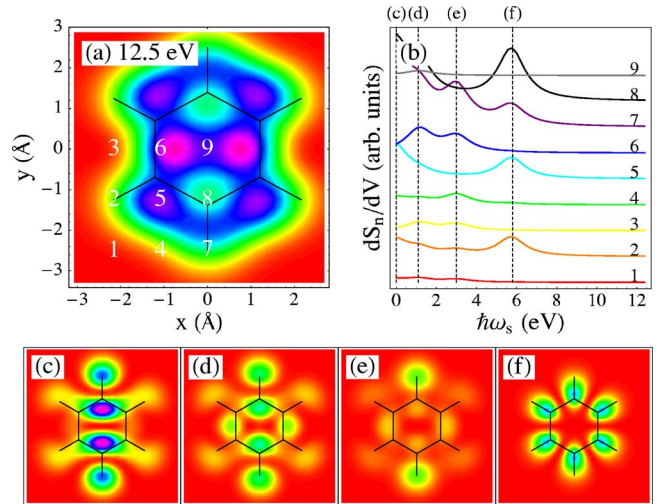


FIG. 7. (Color online) (a) depicts a slice of the local density of states, Eq. (61), of benzene at a bias energy of 12.5 eV . White numbers indicate the lateral position of the tip for the calculated spectra shown in (b) which have been offset for visual clarity. The dashed lines (c)–(f) indicate the energies of the major peaks. Panels (c)–(f) show two-dimensional contour plots of the spatially resolved fluorescence intensity dS_n/dV at a potential bias of $eV=12.5\text{ eV}$ and photon energies $\hbar\omega_s =$ (c) 0.0 , (d) 1.1 , (e) 3.0 , and (f) 5.8 eV . The emission signal is sliced at 1\AA above the molecular plane.

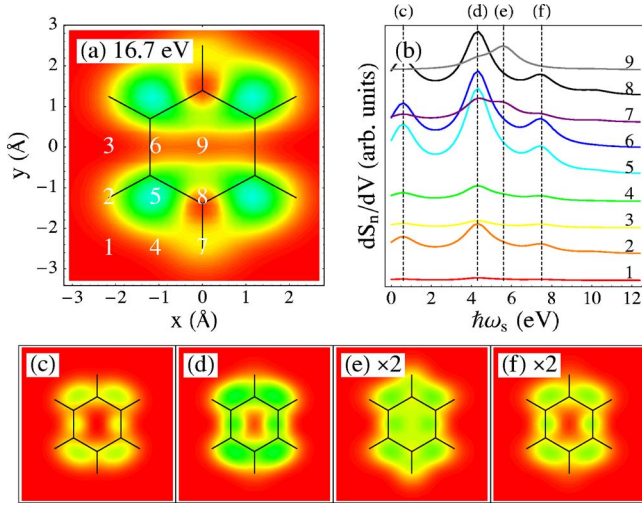


FIG. 8. (Color online) The spatial variation of ρ_{LDOS} , Eq. (61), for benzene at $eV=16.7$ eV is shown in (a) and is plotted on the same scale as Fig. 7(a). (b) shows emission spectra calculated with the tip centered at positions 1–9 indicated in (a). Panels (c)–(f) show the spatial maps (at $z=1$ Å) of the fluorescence peaks at this potential bias and photon energies $\hbar\omega_s$, (c) 0.6, (d) 4.3, (e) 5.6, and (f) 7.5 eV. The signal intensity in (e) and (f) has been scaled by two times in order to enhance the contrast.

clearly seen from the molecular orbital expression Eq. (D4), where the upper limit of the energy integral is then E_F . The coefficient $J_k(\epsilon)$ then represents the transfer matrix element between the filled states of the tip with the unoccupied (higher energy) orbitals of the molecule, which vanishes at zero temperature.

The linewidth Γ , which describes the dephasing rate of many-body states in Eqs. (24)–(26), originates from the electron-electron and electron-phonon interactions in the molecule and interaction with the medium. It can be computed microscopically^{42,43} in terms of the nonequilibrium Green's functions of the molecule.²⁴ This requires a self-consistent calculation for various nonequilibrium Green's functions, Eq. (59). Such a calculation is necessary when the phonon system is out of equilibrium and should lead to excited-state phonon signatures in the fluorescence signal.

ACKNOWLEDGMENTS

The support of the National Science Foundation (Grants No. CHE 0446555, No. EEC-0406750, and No. CHE 0533162) is gratefully acknowledged. We wish to thank Professor Wilson Ho and George Nazin for useful discussions.

APPENDIX A: CORRELATION FUNCTION EXPRESSION FOR FLUORESCENCE

To derive Eq. (2), we treat the emitted photon quantum mechanically and its interaction with the system is described by the Hamiltonian

$$H'_{\text{int}} = a_s B^\dagger + a_s^\dagger B \quad (\text{A1})$$

where $a_s(a_s^\dagger)$ are photon annihilation (creation) field operators for the s th mode with frequency ω_s . These satisfy the boson commutation relation

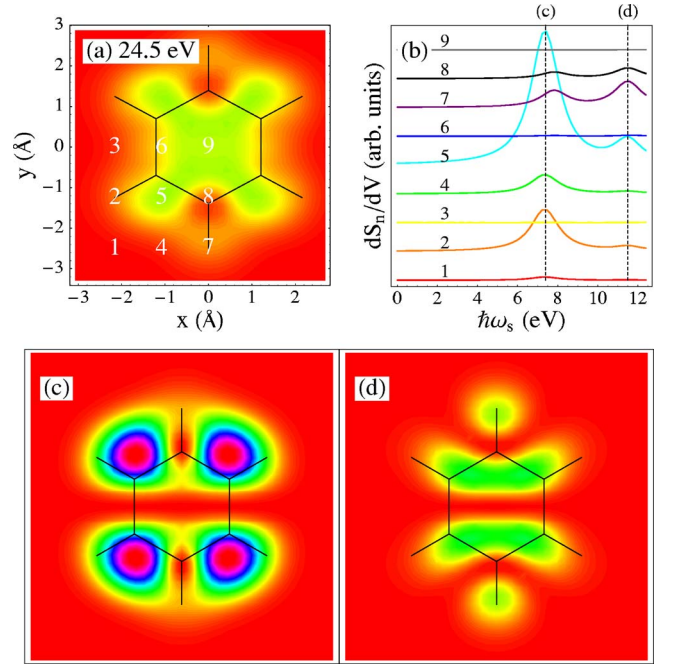


FIG. 9. (Color online) The panels are similar to those shown in Figs. 7 and 8 except that the potential bias energy is set to $eV=24.5$ eV. Only two peaks contribute to the emission spectrum.

$$a_s a_{s'}^\dagger - a_{s'}^\dagger a_s = \delta_{ss'}, \quad a_s^\dagger a_{s'}^\dagger - a_{s'}^\dagger a_s^\dagger = 0, \quad a_s a_{s'} - a_{s'} a_s = 0. \quad (\text{A2})$$

To define the time- and frequency-resolved LIF signal we consider the operator representing the rate of change of the photon occupation of the s 'th mode,²⁶

$$\mathcal{N}_s = \frac{d}{dt} a_s^\dagger a_s = \frac{i}{\hbar} [H'_{\text{int}}, a_s^\dagger a_s] \quad (\text{A3})$$

where H'_{int} is given by Eq. (A1). Using Eqs. (A1) and (A2) in Eq. (A3), we obtain

$$\mathcal{N}_s = \frac{i}{\hbar} (a_s B^\dagger - a_s^\dagger B). \quad (\text{A4})$$

The LIF signal is given by expectation value of \mathcal{N}_s ,

$$S(\omega_s, \omega_L, t) \equiv \langle \mathcal{N}_s \rangle_T = -\frac{2}{\hbar} \text{Im} \{ \langle a_s B^\dagger \rangle_T \} \quad (\text{A5})$$

where $\langle \cdots \rangle_T$ represents the trace with respect to the total density matrix in presence of the incoming and outgoing fields with frequencies ω_L and ω_s , respectively.

We next expand Eq. (A5) to first order in H'_{int} . The time dependence of an interaction picture operator $\tilde{Q}(t)$ is defined as

$$\tilde{Q}(t) = U^\dagger(t, 0) A U(t, 0) \quad (\text{A6})$$

where $U(U^\dagger)$ are the Hilbert space time evolution operators

$$U(t, t_0) = T \exp \left(-\frac{i}{\hbar} \int_{t_0}^t d\tau H_0(\tau) \right)$$

$$U^\dagger(t, t_0) = T^* \exp\left(-\frac{i}{\hbar} \int_{t_0}^t d\tau H_0(\tau)\right). \quad (\text{A7})$$

H_0 is the noninteracting Hamiltonian and $T(T^*)$ is the Hilbert space-time-ordering operator; when acting on a product of operators it rearranges them in increasing order of time from right (left) to left (right). In the interaction picture we get

$$S(\omega_S, \omega_L, t) = -\frac{2}{\hbar} \text{Im} \left[\left\langle T \tilde{a}_s(t) \tilde{B}^\dagger(t) \times \exp\left(-\frac{i}{\hbar} \int_{-\infty}^t d\tau \tilde{\mathcal{L}}_{int}(\tau)\right) \right\rangle_D \right] \quad (\text{A8})$$

where \mathcal{L} is the Liouville operator corresponding to the Hamiltonian H'_{int} and $\langle \cdots \rangle_D$ represents the trace with respect to the density matrix driven by the incoming field. To first order in H'_{int} , which is the lowest order that gives a finite signal, we obtain

$$S(\omega_S, \omega_L, t) = \frac{2}{\hbar^2} \text{Re} \left(\int_{-\infty}^t d\tau [\langle a_s(t) a_s^\dagger(\tau) \rangle_D \langle B^\dagger(t) B(\tau) \rangle_D - \langle a_s^\dagger(\tau) a_s(t) \rangle_D \langle B(\tau) B^\dagger(t) \rangle_D] \right). \quad (\text{A9})$$

Since the scattered mode is initially in the vacuum state, $\langle a_s^\dagger(\tau) a_s(t) \rangle_D = 0$ and $\langle a_s(t) a_s^\dagger(\tau) \rangle_D = e^{-i\omega_S(t-\tau)}$, we obtain

$$S(\omega_S, \omega_L, t) = \frac{2}{\hbar^2} \text{Re} \left(\int_0^\infty d\tau e^{-i\omega_S \tau} \langle B^\dagger(t) B(t-\tau) \rangle_D \right). \quad (\text{A10})$$

Using the time-reversal symmetry $\langle B^\dagger(t) B(t-\tau) \rangle_D^* = \langle B^\dagger(t) B(t+\tau) \rangle_D$,

$$S(\omega_S, \omega_L, t) = \frac{1}{\hbar^2} \int_0^\infty d\tau e^{-i\omega_S \tau} \langle B^\dagger(t) B(t-\tau) \rangle_D + \frac{1}{\hbar^2} \int_0^\infty d\tau e^{i\omega_S \tau} \langle B^\dagger(t) B(t+\tau) \rangle_D \quad (\text{A11})$$

which gives Eq. (2).

APPENDIX B: LIOUVILLE SPACE PATHWAYS FOR CIF

As shown in Fig. 1, Eq. (43) can be separated into three terms representing different time orderings of various super-operators,

$$S_n^I(\omega_S, V, t) = \frac{1}{\hbar^4} \int_0^\infty d\tau \int_{-\infty}^{t-\tau} d\tau_1 \int_{-\infty}^{\tau_1} d\tau_2 \int_{-\infty}^{E_F+eV} d\epsilon \sum_{i < j} \sum_{i' < j'} \sum_{kl} \mu_{ij} \mu_{i'j'} J_k(\epsilon) J_l(\epsilon) \varrho(\epsilon) e^{-i\omega_S \tau} e^{-(i\hbar)\epsilon(\tau_1-\tau_2)} \times \langle \tilde{\psi}_{j'R}^\dagger(t) \tilde{\psi}_{i'R}(t) \tilde{\psi}_{iL}^\dagger(t-\tau) \tilde{\psi}_{jL}(t-\tau) \tilde{\psi}_{kL}^\dagger(\tau_1) \tilde{\psi}_{lR}(\tau_2) \rangle, \quad (\text{B1})$$

$$S_n^{II}(\omega_S, V, t) = \frac{1}{\hbar^4} \int_0^\infty d\tau \int_{-\infty}^{t-\tau} d\tau_2 \int_{-\infty}^{\tau_2} d\tau_1 \int_{-\infty}^{E_F+eV} d\epsilon \sum_{i < j} \sum_{i' < j'} \sum_{kl} \mu_{ij} \mu_{i'j'} J_k(\epsilon) J_l(\epsilon) \varrho(\epsilon) e^{-i\omega_S \tau} e^{-(i\hbar)\epsilon(\tau_1-\tau_2)} \times \langle \tilde{\psi}_{j'R}^\dagger(t) \tilde{\psi}_{i'R}(t) \tilde{\psi}_{iL}^\dagger(t-\tau) \tilde{\psi}_{jL}(t-\tau) \tilde{\psi}_{lR}(\tau_2) \tilde{\psi}_{kL}^\dagger(\tau_1) \rangle, \quad (\text{B2})$$

$$S_n^{III}(\omega_S, V, t) = \frac{1}{\hbar^4} \int_{-\infty}^t d\tau_2 \int_{t-\tau_2}^\infty d\tau \int_{-\infty}^{t-\tau} d\tau_1 \int_{-\infty}^{E_F+eV} d\epsilon \sum_{i < j} \sum_{i' < j'} \sum_{kl} \mu_{ij} \mu_{i'j'} J_k(\epsilon) J_l(\epsilon) \varrho(\epsilon) e^{-i\omega_S \tau} e^{-(i\hbar)\epsilon(\tau_1-\tau_2)} \times \langle \tilde{\psi}_{j'R}^\dagger(t) \tilde{\psi}_{i'R}(t) \tilde{\psi}_{lR}(\tau_2) \tilde{\psi}_{iL}^\dagger(t-\tau) \tilde{\psi}_{jL}(t-\tau) \tilde{\psi}_{kL}^\dagger(\tau_1) \rangle. \quad (\text{B3})$$

Equations (B1)–(B3) are analogous to Eqs. (14)–(16). Note that they do not include the time-ordering operator explicitly.

Making the change of variables $\tau = t_1$, $\tau_1 = t - t_1 - t_2$, $\tau_2 = t - t_1 - t_2 - t_3$ in Eq. (B1), we obtain

$$S_n^I(\omega_S, V, t) = \frac{1}{\hbar^4} \int_0^\infty dt_1 \int_0^\infty dt_2 \int_0^\infty dt_3 \int_{-\infty}^{E_F+eV} d\epsilon \sum_{i < j} \sum_{i' < j'} \sum_{kl} \mu_{ij} \mu_{i'j'} J_k(\epsilon) J_l(\epsilon) \varrho(\epsilon) e^{-i\omega_S t_1} e^{-(i\hbar)\epsilon t_3} \times \langle \tilde{\psi}_{j'R}^\dagger(t) \tilde{\psi}_{i'R}(t) \tilde{\psi}_{iL}^\dagger(t-t_1) \tilde{\psi}_{jL}(t-t_1) \tilde{\psi}_{kL}^\dagger(t-t_1-t_2) \tilde{\psi}_{lR}(t-t_1-t_2-t_3) \rangle. \quad (\text{B4})$$

Similarly, substituting $\tau = t_1$, $\tau_2 = t - t_1 - t_2$, $\tau_1 = t - t_1 - t_2 - t_3$ in Eq. (B2) gives

$$S_n^I(\omega_S, V, t) = \frac{1}{\hbar^4} \int_0^\infty dt_1 \int_0^\infty dt_2 \int_0^\infty dt_3 \int_{-\infty}^{E_F+eV} d\epsilon \sum_{i<j} \sum_{i'<j'} \sum_{kl} \mu_{ij} \mu_{i'j'} J_k(\epsilon) J_l(\epsilon) \varrho(\epsilon) e^{-i\omega_S t_1} e^{(i\hbar)\epsilon t_3} \\ \times \langle \tilde{\psi}_{j'R}^\dagger(t) \tilde{\psi}_{i'R}(t) \tilde{\psi}_{iR}(t-t_1-t_2) \tilde{\psi}_{iL}^\dagger(t-t_1) \tilde{\psi}_{jL}(t-t_1) \tilde{\psi}_{kL}^\dagger(t-t_1-t_2-t_3) \rangle \quad (\text{B5})$$

and in Eq. (B3), we substitute $\tau=t_2-t_1$, $\tau_1=t-t_1-t_3$, $\tau_2=t-t_2$, to get

$$S_n^{III}(\omega_S, V, t) = \frac{1}{\hbar^4} \int_0^\infty dt_1 \int_0^\infty dt_2 \int_0^\infty dt_3 \int_{-\infty}^{E_F+eV} d\epsilon \sum_{i<j} \sum_{i'<j'} \sum_{kl} \mu_{ij} \mu_{i'j'} J_k(\epsilon) J_l(\epsilon) \varrho(\epsilon) e^{-i\omega_S(t_1+t_2)} e^{-(i\hbar)\epsilon(t_2+t_3)} \\ \times \langle \tilde{\psi}_{j'R}^\dagger(t) \tilde{\psi}_{i'R}(t) \tilde{\psi}_{iR}(t-t_3) \tilde{\psi}_{iL}^\dagger(t-t_1-t_2) \tilde{\psi}_{jL}(t-t_1-t_2) \tilde{\psi}_{kL}^\dagger(t-t_1-t_2-t_3) \rangle. \quad (\text{B6})$$

Hilbert space expressions for S_n^I , S_n^{II} , and S_n^{III} can be obtained by substituting

$$\langle \tilde{\psi}_{j'R}^\dagger(t) \tilde{\psi}_{i'R}(t) \tilde{\psi}_{iL}^\dagger(t-t_1) \tilde{\psi}_{jL}(t-t_1) \\ \times \tilde{\psi}_{kL}^\dagger(t-t_1-t_2) \tilde{\psi}_{iR}(t-t_1-t_2-t_3) \rangle \\ \equiv \langle \tilde{\psi}_j(t-t_1-t_2-t_3) \tilde{\psi}_{j'}^\dagger(t) \tilde{\psi}_{i'}(t) \tilde{\psi}_i^\dagger(t-t_1) \tilde{\psi}_j(t-t_1) \\ \times \tilde{\psi}_k^\dagger(t-t_1-t_2) \rangle, \quad (\text{B7})$$

$$\langle \tilde{\psi}_{j'R}^\dagger(t) \tilde{\psi}_{i'R}(t) \tilde{\psi}_{iL}^\dagger(t-t_1) \tilde{\psi}_{jL}(t-t_1) \tilde{\psi}_{iR}(t-t_1-t_2) \\ \times \tilde{\psi}_{kL}^\dagger(t-t_1-t_2-t_3) \rangle \\ \equiv \langle \tilde{\psi}_j(t-t_1-t_2) \tilde{\psi}_{j'}^\dagger(t) \tilde{\psi}_{i'}(t) \tilde{\psi}_i^\dagger(t-t_1) \tilde{\psi}_j(t-t_1) \\ \times \tilde{\psi}_k^\dagger(t-t_1-t_2-t_3) \rangle, \quad (\text{B8})$$

$$\langle \tilde{\psi}_{j'R}^\dagger(t) \tilde{\psi}_{i'R}(t) \tilde{\psi}_{iR}(t-t_3) \tilde{\psi}_{iL}^\dagger(t-t_1-t_2) \tilde{\psi}_{jL}(t-t_1-t_2) \\ \times \tilde{\psi}_{kL}^\dagger(t-t_1-t_2-t_3) \rangle \\ \equiv \langle \tilde{\psi}_j(t-t_3) \tilde{\psi}_{j'}^\dagger(t) \tilde{\psi}_{i'}(t) \tilde{\psi}_i^\dagger(t-t_1-t_2) \\ \times \tilde{\psi}_j(t-t_1-t_2) \tilde{\psi}_k^\dagger(t-t_1-t_2-t_3) \rangle. \quad (\text{B9})$$

Making these substitutions and taking the derivative with respect to the applied bias V gives Eqs. (44)–(46).

APPENDIX C: EXPANDING CIF IN MANY-BODY STATES

As was done in Eq. (23), we insert the many-body states into Eq. (B7) and substitute in Eq. (B4) to get

$$S_n^I(\omega_S, V, t) = \frac{1}{\hbar^4} \sum_{i<j} \sum_{i'<j'} \sum_{kl} \sum_{abcd} P(a) \langle a | \psi_i | b \rangle \langle b | \psi_{j'}^\dagger, \psi_{i'} | c \rangle \\ \times \langle c | \psi_i^\dagger \psi_j | d \rangle \langle d | \psi_k^\dagger | a \rangle \mu_{ij} \mu_{i'j'} \\ \times \int_0^\infty dt_1 \int_0^\infty dt_2 \int_0^\infty dt_3 \int_{-\infty}^{E_F+eV} d\epsilon J_k(\epsilon) J_l(\epsilon)$$

$$\times e^{i(\omega_{bc}-\omega_S+i\Gamma_{bc})t_1} e^{i(\omega_{bd}+i\Gamma_{bd})t_2} e^{(i\hbar)(\hbar\omega_{ba}-\epsilon+i\Gamma_{ba})t_3} \quad (\text{C1})$$

where $\langle a | \tilde{\psi}(t) | b \rangle = \langle a | \psi | b \rangle e^{-i(\omega_{ba}+i\Gamma_{ba})t}$, etc.

The time integrals in Eq. (C1) can now be performed to get

$$S_n^I(\omega_S, V) = -\frac{i}{\hbar^3} \sum_{i<j} \sum_{i'<j'} \sum_{kl} \sum_{abcd} P(a) \langle a | \psi_i | b \rangle \langle b | \psi_{j'}^\dagger, \psi_{i'} | c \rangle \\ \times \langle c | \psi_i^\dagger \psi_j | d \rangle \langle d | \psi_k^\dagger | a \rangle \mu_{ij} \mu_{i'j'} \\ \times \frac{1}{(\omega_{bc}-\omega_S+i\Gamma_{bc})(\omega_{bd}+i\Gamma_{bd})} \\ \times \int_{-\infty}^{E_F+eV} d\epsilon \frac{J_k(\epsilon) J_l(\epsilon)}{\hbar\omega_{ba}-\epsilon+i\Gamma_{ba}}. \quad (\text{C2})$$

Following similar steps, we get for S_n^{II} and S_n^{III}

$$S_n^{II}(\omega_S, V) = -\frac{i}{\hbar^3} \sum_{i<j} \sum_{i'<j'} \sum_{kl} \sum_{abcd} P(a) \langle a | \psi_i | b \rangle \langle b | \psi_{j'}^\dagger, \psi_{i'} | c \rangle \\ \times \langle c | \psi_i^\dagger \psi_j | d \rangle \langle d | \psi_k^\dagger | a \rangle \mu_{ij} \mu_{i'j'} \\ \times \frac{1}{(\omega_{bc}-\omega_S+i\Gamma_{bc})(\omega_{bd}+i\Gamma_{bd})} \\ \times \int_{-\infty}^{E_F+eV} d\epsilon \frac{J_k(\epsilon) J_l(\epsilon)}{\epsilon-\hbar\omega_{da}+i\Gamma_{da}}, \quad (\text{C3})$$

$$S_n^{III}(\omega_S, V)$$

$$= -\frac{i}{\hbar^2} \sum_{i<j} \sum_{i'<j'} \sum_{kl} \sum_{abcd} P(a) \langle a | \psi_i | b \rangle \langle b | \psi_{j'}^\dagger, \psi_{i'} | c \rangle \langle c | \psi_i^\dagger \psi_j | d \rangle \\ \times \langle d | \psi_k^\dagger | a \rangle \mu_{ij} \mu_{i'j'} \frac{1}{(\omega_{bc}-\omega+i\Gamma_{bc})} \\ \times \int_{-\infty}^{E_F+eV} d\epsilon \frac{J_k(\epsilon) J_l(\epsilon)}{(\hbar\omega_{ac}-\hbar\omega_S+\epsilon+i\Gamma_{ac})(\epsilon-\hbar\omega_{da}+i\Gamma_{da})}. \quad (\text{C4})$$

In the absence of dephasing, the total signal from a nega-

tively charged molecule, $\mathcal{S}_n(\omega) = 2\text{Re}[\mathcal{S}_n^I(\omega) + \mathcal{S}_n^{II}(\omega) + \mathcal{S}_n^{III}(\omega)]$, is given by

$$\begin{aligned} \mathcal{S}_n(\omega, V) = & \frac{2\pi}{\hbar} \sum_{ac} P(a) \int_{-\infty}^{E_F + eV} d\epsilon \\ & \times \left| \sum_{i < j} \sum_k \sum_b \frac{\mu_{ij} \langle a | \psi_k | b \rangle \langle b | \psi_i^\dagger | c \rangle J_k(\epsilon)}{\epsilon - \hbar\omega_{ba} + i\eta} \right|^2 \\ & \times \delta(\hbar\omega_S + \hbar\omega_{ca} - \epsilon). \end{aligned} \quad (\text{C5})$$

Taking the derivative of Eq. (C5) with respect to V gives Eq. (47).

APPENDIX D: DERIVATION OF EQS. (55) and (56)

Using Eq. (54) in (B1) and substituting in Eq. (B7) we obtain

$$\mathcal{S}_I(\omega_S, V) = \frac{i}{\hbar} \sum_{i < j, j'}^{\text{unocc}} \sum_{jj'}^{\text{unocc}} \frac{\mu_{ij} \mu_{ij'}}{(\epsilon_{j'} - \epsilon_i - \hbar\omega_S + i\Gamma_{j'i})(\epsilon_{j'} - \epsilon_j + i\Gamma_{j'j})} \int_{-\infty}^{E_F + eV} d\epsilon \frac{J_j(\epsilon) J_{j'}(\epsilon) \varrho(\epsilon)}{\epsilon_{j'} - \epsilon + i\Gamma_{j'e}} \quad (\text{D1})$$

where the sum over i, j, j' runs over all unoccupied orbitals and Γ_{ij} is the dephasing rate between orbitals i and j . Γ_{ϵ_j} inside the integral represents the dephasing rate between the j th molecular orbital and the tip state with energy ϵ . Similarly for \mathcal{S}_{II} and \mathcal{S}_{III} , we obtain

$$\mathcal{S}_{II}(\omega_S, V) = \frac{i}{\hbar} \sum_{i < j, j'}^{\text{unocc}} \sum_{jj'}^{\text{unocc}} \frac{\mu_{ij} \mu_{ij'}}{(\epsilon_{j'} - \epsilon_i - \hbar\omega_S + i\Gamma_{j'i})(\epsilon_{j'} - \epsilon_j + i\Gamma_{j'j})} \int_{-\infty}^{E_F + eV} d\epsilon \frac{J_j(\epsilon) J_{j'}(\epsilon) \varrho(\epsilon)}{\epsilon - \epsilon_j + i\Gamma_{\epsilon_j}}, \quad (\text{D2})$$

$$\mathcal{S}_{III}(\omega_S, V) = \frac{i}{\hbar} \sum_{i < j, j'}^{\text{unocc}} \sum_{jj'}^{\text{unocc}} \frac{\mu_{ij} \mu_{ij'}}{\epsilon_{j'} - \epsilon_i - \hbar\omega_S + i\Gamma_{j'i}} \int_{-\infty}^{E_F + eV} d\epsilon \frac{J_j(\epsilon) J_{j'}(\epsilon) \varrho(\epsilon)}{(\epsilon - \epsilon_i - \hbar\omega_S + i\Gamma_{\epsilon_i})(\epsilon - \epsilon_j + i\Gamma_{\epsilon_j})}. \quad (\text{D3})$$

The total signal is

$$\mathcal{S}_n(\omega_S, V) = \frac{2}{\hbar} \text{Im} \sum_{i < j, j'}^{\text{unocc}} \sum_{jj'}^{\text{unocc}} \mu_{ij} \mu_{ij'} \int_{-\infty}^{E_F + eV} d\epsilon \frac{J_j(\epsilon) J_{j'}(\epsilon) \varrho(\epsilon)}{(\epsilon - \epsilon_j + i\Gamma_{\epsilon_j})(\epsilon_{j'} - \epsilon + i\Gamma_{j'e})(\epsilon - \epsilon_i - \hbar\omega_S + i\Gamma_{\epsilon_i})}. \quad (\text{D4})$$

Similar expressions are obtained for the signal \mathcal{S}_p from a positive molecule,

$$\mathcal{S}_p(\omega_S, V) = \frac{2}{\hbar} \text{Im} \sum_{i < j}^{\text{occ}} \sum_{i' < j'}^{\text{occ}} \sum_J^{\text{occ}} \mu_{ij} \mu_{i'j'} \int_{E_F + eV}^{\infty} d\epsilon \frac{J_i(\epsilon) J_{i'}(\epsilon) \varrho(\epsilon)}{(\epsilon_i - \epsilon + i\Gamma_{i\epsilon})(\epsilon - \epsilon_{i'} + i\Gamma_{\epsilon i'}) (\epsilon_j - \epsilon - \hbar\omega_S + i\Gamma_{j\epsilon})}. \quad (\text{D5})$$

Taking the derivative of Eqs. (D4) and (D5), with respect to V gives Eqs. (55) and (56), respectively.

APPENDIX E: GREEN'S FUNCTION EXPRESSIONS FOR CIF

Adopting the electron gas model for the molecule, the trace of the product of six Fermi operators in Eq. (38) taken over the molecular density matrix can be expressed in terms of the products of averages of pairs of operators using the superoperator Wick's theorem,²⁵

$$\begin{aligned} \langle \mathcal{T} \psi_{iL}^\dagger(t - \tau) \psi_{jL}(t - \tau) \psi_{j'R}^\dagger(t) \psi_{i'R}(t) \psi_{kL}^\dagger(\tau_1) \psi_{iR}(\tau_2) \rangle_0 = & \langle \mathcal{T} \psi_{iL}^\dagger(t - \tau) \psi_{jL}(t - \tau) \rangle_0 [\langle \mathcal{T} \psi_{j'R}^\dagger(t) \psi_{i'R}(t) \rangle_0 \langle \mathcal{T} \psi_{kL}^\dagger(\tau_1) \psi_{iR}(\tau_2) \rangle_0 \\ & + \langle \mathcal{T} \psi_{j'R}^\dagger(t) \psi_{iR}(\tau_2) \rangle_0 \langle \mathcal{T} \psi_{i'R}(t) \psi_{kL}^\dagger(\tau_1) \rangle_0] \langle \mathcal{T} \psi_{iL}^\dagger(t - \tau) \psi_{i'R}(t) \rangle_0 \\ & \times [\langle \mathcal{T} \psi_{jL}(t - \tau) \psi_{j'R}^\dagger(t) \rangle_0 \langle \mathcal{T} \psi_{kL}^\dagger(\tau_1) \psi_{iR}(\tau_2) \rangle_0 - \langle \mathcal{T} \psi_{jL}(t - \tau) \psi_{kL}^\dagger(\tau_1) \rangle_0 \\ & \times \langle \mathcal{T} \psi_{j'R}^\dagger(t) \psi_{iR}(\tau_2) \rangle_0] + \langle \mathcal{T} \psi_{iL}^\dagger(t - \tau) \psi_{iR}(\tau_2) \rangle_0 \\ & \times [\langle \mathcal{T} \psi_{jL}(t - \tau) \psi_{j'R}^\dagger(t) \rangle_0 \langle \mathcal{T} \psi_{i'R}(t) \psi_{kL}^\dagger(\tau_1) \rangle_0 \\ & + \langle \mathcal{T} \psi_{jL}(t - \tau) \psi_{kL}^\dagger(\tau_1) \rangle_0 \langle \mathcal{T} \psi_{j'R}^\dagger(t) \psi_{i'R}(t) \rangle_0] \end{aligned} \quad (\text{E1})$$

where $\langle \cdots \rangle_0$ denotes that the trace is with respect to the noninteracting density matrix.

Using the Liouville space Green's function

$$G_{\alpha\beta}^{ij}(t_1, t_2) = -\frac{i}{\hbar} \langle T \psi_{i\alpha}(t_1) \psi_{j\beta}^\dagger(t_2) \rangle, \quad \alpha, \beta = L, R. \quad (\text{E2})$$

Equation (38) can be factorized as

$$\begin{aligned} \mathcal{S}_n(\omega, t) = & \int_{-\infty}^{\infty} d\tau \int_{-\infty}^{t-\tau} d\tau_1 \int_{-\infty}^t d\tau_2 e^{-i\omega_S \tau} \sum_{i < j} \sum_{i' < j'} \sum_{kl} \sum_{\mu\nu} \mu_{ij} \mu_{i'j'} J_{k\mu} J_{l\nu} G_{LR}^{\mu\nu}(\tau_1, \tau_2) \{ G_{LL}^{0ji}(t - \tau, t^+ - \tau^+) [G_{RR}^{0i'j'}(t, t^+) G_{RL}^{0lk}(\tau_2, \tau_1) \\ & - G_{RR}^{0lj'}(\tau_2, t) G_{RL}^{0i'k}(t, \tau_1)] - G_{RL}^{0i'i}(t, t - \tau) [G_{LR}^{0jj'}(t - \tau, t) G_{RL}^{0lk}(\tau_2, \tau_1) - G_{LL}^{0jk}(t - \tau, \tau_1) G_{RR}^{0lj'}(\tau_2, t)] + G_{RL}^{0li}(\tau_2, t - \tau) \\ & \times [G_{LR}^{0jj'}(t - \tau, t) G_{RL}^{0i'k}(t, \tau_1) - G_{LL}^{0jk}(t - \tau, \tau_1) G_{RR}^{0i'j'}(t, t^+)] \}. \end{aligned} \quad (\text{E3})$$

Similarly, we obtain for \mathcal{S}_p ,

$$\begin{aligned} \mathcal{S}_p(\omega_S, V, t) = & \int_{-\infty}^{\infty} d\tau \int_{-\infty}^{t-\tau} d\tau_1 \int_{-\infty}^t d\tau_2 e^{-i\omega_S \tau} \sum_{i < j} \sum_{i' < j'} \sum_{kl} \sum_{\mu\nu} \mu_{ij} \mu_{i'j'} J_{k\mu} J_{l\nu} G_{\nu\mu}^>(\tau_2, \tau_1) \{ G_{LL}^{0ji}(t - \tau, t^+ - \tau^+) [G_{RR}^{0i'j'}(t, t^+) G_{LR}^{0kl}(\tau_1, \tau_2) \\ & - G_{LR}^{0kj'}(\tau_1, t) G_{RR}^{0i'l}(t, \tau_2)] - G_{RL}^{0i'i}(t, t - \tau) [G_{LR}^{0jj'}(t - \tau, t) G_{LR}^{0kl}(\tau_1, \tau_2) + G_{LR}^{0jl}(t - \tau, \tau_2) G_{LR}^{0kj'}(\tau, t)] + G_{LL}^{0ki}(\tau_1, t - \tau) \\ & \times [G_{LR}^{0jj'}(t - \tau, t) G_{RR}^{0i'l}(t, \tau_2) - G_{LR}^{0il}(t - \tau, \tau_2) G_{RR}^{0i'j'}(t, t^+)] \}. \end{aligned} \quad (\text{E4})$$

Each superoperator Green's function corresponds to one of the Keldysh Green's functions in Hilbert space.^{21,25} Replacing the Liouville space Green's functions with their Hilbert space counterparts,

$$G_{LL}^{ij}(t_1, t_2) = G_{ij}^T(t_1, t_2), \quad G_{RR}^{ij}(t_1, t_2) = -G_{ij}^{\bar{T}}(t_1, t_2)$$

$$G_{LR}^{ij}(t_1, t_2) = G_{ij}^<(t_1, t_2), \quad G_{RL}^{ij}(t_1, t_2) = -G_{ij}^>(t_1, t_2), \quad (\text{E5})$$

where G^T , $G^{\bar{T}}$, $G^<$, and $G^>$ are, respectively, time-ordered, anti-time-ordered, lesser, and greater Green's functions in Hilbert space,^{18,19} we obtain

$$\begin{aligned} \mathcal{S}_n(\omega_S, t) = & \int_{-\infty}^{\infty} d\tau \int_{-\infty}^{t-\tau} d\tau_1 \int_{-\infty}^t d\tau_2 e^{-i\omega_S \tau} \sum_{i < j} \sum_{i' < j'} \sum_{kl} \sum_{\mu\nu} \mu_{ij} \mu_{i'j'} J_{k\mu} J_{l\nu} G_{\nu\mu}^<(\tau_1, \tau_2) \{ G_{ji}^{0T}(t - \tau, t^+ - \tau^+) [G_{i'j'}^{\bar{T}}(t, t^+) G_{lk}^{0>}(\tau_2, \tau_1) \\ & - G_{i'j'}^{\bar{T}}(\tau_2, t) G_{i'k}^{0>}(t, \tau_1)] - G_{i'i}^{0>}(t, t - \tau) [G_{jj'}^{0<}(t - \tau, t) G_{lk}^{0>}(\tau_2, \tau_1) - G_{jk}^{0T}(t - \tau, \tau_1) G_{i'j'}^{\bar{T}}(\tau_2, t)] \\ & + G_{li}^{0>}(\tau_2, t - \tau) [G_{jj'}^{0<}(t - \tau, t) G_{i'k}^{0>}(t, \tau_1) - G_{jk}^{0T}(t - \tau, \tau_1) G_{i'j'}^{\bar{T}}(t, t^+)] \}, \end{aligned} \quad (\text{E6})$$

where a 0 superscript denotes that the trace is taken with respect to the density matrix of the noninteracting molecule. Note that the tip Green's function $G_{\nu\mu}^<$ involves all many-body interactions. Similarly, for a positively charged molecule we obtain

$$\begin{aligned} \mathcal{S}_p(\omega_S, V, t) = & \int_{-\infty}^{\infty} d\tau \int_{-\infty}^{t-\tau} d\tau_1 \int_{-\infty}^t d\tau_2 e^{-i\omega_S \tau} \sum_{i < j} \sum_{i' < j'} \sum_{kl} \sum_{\mu\nu} \mu_{ij} \mu_{i'j'} J_{k\mu} J_{l\nu} G_{\nu\mu}^>(\tau_2, \tau_1) \{ G_{i'i}^{0>}(t, t - \tau) [G_{jj'}^{0<}(t - \tau, t) G_{kl}^{0<}(\tau_1, \tau_2) \\ & + G_{jl}^{0<}(t - \tau, \tau_2) G_{kj'}^{0<}(\tau, t)] - G_{ji}^{0T}(t - \tau, t^+ - \tau^+) [G_{i'j'}^{\bar{T}}(t, t^+) G_{kl}^<(\tau_1, \tau_2) - G_{kj'}^{0<}(\tau_1, t) G_{i'l}^{\bar{T}}(\tau_2, t)] \\ & - G_{ki}^{0T}(\tau_1, t - \tau) [G_{jj'}^{0<}(t - \tau, t) G_{i'l}^{\bar{T}}(\tau_2, t) - G_{jl}^{0<}(t - \tau, \tau_2) G_{i'j'}^{\bar{T}}(t, t^+)] \}. \end{aligned} \quad (\text{E7})$$

Assuming the free electron gas model for the tip, we can replace the tip Green's functions $G^<$ and $G^>$ using Eqs. (41) and (51), respectively. This gives

$$\begin{aligned} \mathcal{S}_n(\omega_S, t) = & \frac{i}{\hbar} \int_{-\infty}^{\infty} d\tau \int_{-\infty}^{t-\tau} d\tau_1 \int_{-\infty}^t d\tau_2 \int_{-\infty}^{E_F + eV} d\epsilon \varrho(\epsilon) e^{-i\omega_S \tau} \sum_{i < j} \sum_{i' < j'} \sum_{kl} \mu_{ij} \mu_{i'j'} J_k(\epsilon) J_l(\epsilon) e^{-i\epsilon(\tau_1 - \tau_2)} \{ G_{ji}^{0T}(t - \tau, t^+ - \tau^+) \\ & \times [G_{i'j'}^{\bar{T}}(t, t^+) G_{lk}^{0>}(\tau_2, \tau_1) - G_{i'j'}^{\bar{T}}(\tau_2, t) G_{i'k}^{0>}(t, \tau_1)] - G_{i'i}^{0>}(t, t - \tau) [G_{jj'}^{0<}(t - \tau, t) G_{lk}^{0>}(\tau_2, \tau_1) - G_{jk}^{0T}(t - \tau, \tau_1) G_{i'j'}^{\bar{T}}(\tau_2, t)] \\ & + G_{li}^{0>}(\tau_2, t - \tau) [G_{jj'}^{0<}(t - \tau, t) G_{i'k}^{0>}(t, \tau_1) - G_{jk}^{0T}(t - \tau, \tau_1) G_{i'j'}^{\bar{T}}(t, t^+)] \}, \end{aligned} \quad (\text{E8})$$

$$\begin{aligned}
\mathcal{S}_p(\omega_S, V, t) = & -\frac{i}{\hbar} \int_{-\infty}^{\infty} d\tau \int_{-\infty}^{t-\tau} d\tau_1 \int_{-\infty}^t d\tau_2 \int_{E_F+eV}^{\infty} d\epsilon \varrho(\epsilon) e^{-i\omega_S \tau} \sum_{i < j} \sum_{i' < j'} \sum_{kl} \mu_{ij} \mu_{i'j'} J_k(\epsilon) J_l(\epsilon) e^{-(i\hbar)\epsilon(\tau_2-\tau_1)} \\
& \times \{G_{i'i}^{0>}(t, t-\tau) [G_{jj'}^{0<}(t-\tau, t) G_{kl}^{0<}(\tau_1, \tau_2) + G_{jl}^{0<}(t-\tau, \tau_2) G_{kj'}^{0<}(\tau, t)] - G_{ji}^{0T}(t-\tau, t^+ - \tau^+) [G_{i'j'}^{0\tilde{T}}(t, t^+) G_{kl}^{0<}(\tau_1, \tau_2) \\
& - G_{kj'}^{0<}(\tau_1, t) G_{i'l}^{0\tilde{T}}(t, \tau_2)] - G_{ki}^{0T}(\tau_1, t-\tau) [G_{jj'}^{0<}(t-\tau, t) G_{i'l}^{0\tilde{T}}(t, \tau_2) - G_{jl}^{0<}(t-\tau, \tau_2) G_{i'j'}^{0\tilde{T}}(t, t^+)]\}. \tag{E9}
\end{aligned}$$

Taking the derivative of Eqs. (E8) and (E9) with respect to the bias V , we obtain

$$\begin{aligned}
\frac{d\mathcal{S}_n}{dV}(\omega_S, V, t) = & \frac{ie}{\hbar} \int_{-\infty}^{\infty} d\tau \int_{-\infty}^{t-\tau} d\tau_1 \int_{-\infty}^t d\tau_2 \varrho(E_F + eV) e^{-i\omega_S \tau} \sum_{i < j} \sum_{i' < j'} \sum_{kl} \mu_{ij} \mu_{i'j'} J_k(E_F + eV) J_l(E_F + eV) e^{-(i\hbar)(E_F+eV)(\tau_1-\tau_2)} \\
& \times \{G_{ji}^{0T}(t-\tau, t^+ - \tau^+) [G_{i'j'}^{0\tilde{T}}(t, t^+) G_{lk}^{0>}(\tau_2, \tau_1) - G_{lj'}^{0\tilde{T}}(\tau_2, t) G_{i'k}^{0>}(t, \tau_1)] - G_{i'i}^{0>}(t, t-\tau) [G_{jj'}^{0<}(t-\tau, t) G_{lk}^{0>}(\tau_2, \tau_1) \\
& - G_{jk}^{0T}(t-\tau, \tau_1) G_{i'l}^{0\tilde{T}}(\tau_2, t)] + G_{li}^{0>}(\tau_2, t-\tau) [G_{jj'}^{0<}(t-\tau, t) G_{i'k}^{0>}(t, \tau_1) - G_{jk}^{0T}(t-\tau, \tau_1) G_{i'j'}^{0\tilde{T}}(t, t^+)]\}, \tag{E10}
\end{aligned}$$

$$\begin{aligned}
\frac{d\mathcal{S}_p}{dV}(\omega_S, V, t) = & -\frac{ie}{\hbar} \int_{-\infty}^{\infty} d\tau \int_{-\infty}^{t-\tau} d\tau_1 \int_{-\infty}^t d\tau_2 \varrho(E_F + eV) e^{-i\omega_S \tau} \sum_{i < j} \sum_{i' < j'} \sum_{kl} \mu_{ij} \mu_{i'j'} J_k(E_F + eV) J_l(E_F + eV) e^{-(i\hbar)(E_F+eV)(\tau_2-\tau_1)} \\
& \times \{G_{i'i}^{0>}(t, t-\tau) [G_{jj'}^{0<}(t-\tau, t) G_{kl}^{0<}(\tau_1, \tau_2) + G_{jl}^{0<}(t-\tau, \tau_2) G_{kj'}^{0<}(\tau, t)] - G_{ji}^{0T}(t-\tau, t^+ - \tau^+) [G_{i'j'}^{0\tilde{T}}(t, t^+) G_{kl}^{0<}(\tau_1, \tau_2) \\
& - G_{kj'}^{0<}(\tau_1, t) G_{i'l}^{0\tilde{T}}(t, \tau_2)] - G_{ki}^{0T}(\tau, t-\tau) [G_{jj'}^{0<}(t-\tau, t) G_{i'l}^{0\tilde{T}}(t, \tau_2) - G_{jl}^{0<}(t-\tau, \tau_2) G_{i'j'}^{0\tilde{T}}(t, t^+)]\}. \tag{E11}
\end{aligned}$$

Transforming in the frequency domain, we obtain Eqs. (57) and (58).

-
- ¹J. S. Kim, I. Grizzi, J. H. Burroughes, and R. H. Friend, *Appl. Phys. Lett.* **87**, 023506 (2005); A. J. A. B. Seeley, R. H. Friend, J. H. Burroughes, and J. S. Kim, *J. Appl. Phys.* **96**, 7643 (2004); A. Hayer, A. Köhler, E. Arisi, I. Bergenti, A. Dediu, C. Taliani, M. Al-Suti, and M. S. Khan, *Synth. Met.* **147**, 155 (2004).
- ²X. H. Qiu, G. V. Nazin, and W. Ho, *Science* **299**, 542 (2003); G. V. Nazin, X. H. Qiu, and W. Ho, *Phys. Rev. Lett.* **90**, 216110 (2003).
- ³J. A. Misewich, R. Martel, Ph. Avouris, J. C. Tsang, S. Heinze and J. Tersoff, *Science* **300**, 783 (2003).
- ⁴X. Duan, Y. Huang, Y. Cui, J. Wong, and C. M. Lieber, *Nature (London)* **409**, 66 (2001).
- ⁵A. Tikhonov, R. D. Coalson, and Y. Dohnovsky, *J. Chem. Phys.* **116**, 10909 (2002); **117**, 567 (2003).
- ⁶J. Lehmann, S. Kohler, P. Hanggi, and A. Nitzan, *Phys. Rev. Lett.* **88**, 228305 (2002).
- ⁷E. R. Bittner, S. Karabunarliev, and A. Ye, *J. Chem. Phys.* **122**, 034707 (2005).
- ⁸A. Nitzan, *Annu. Rev. Phys. Chem.* **52**, 681 (2001).
- ⁹A. Nitzan and M. A. Ratner, *Science* **300**, 1384 (2003).
- ¹⁰T. Mii, S. Tikhodeev, and H. Ueba, *Surf. Sci.* **502**, 26 (2002); *Phys. Rev. B* **68**, 205406 (2003).
- ¹¹N. D. Lang, *Phys. Rev. B* **52**, 5335 (1995).
- ¹²S.-H. Ke, H. U. Baranger, and W. Yang, *Phys. Rev. B* **70**, 085410 (2004).
- ¹³J. Taylor, H. Guo, and J. Wang, *Phys. Rev. B* **63**, 245407 (2001).
- ¹⁴A. Pecchia and A. Di Carlo, *Rep. Prog. Phys.* **67**, 1497 (2004).
- ¹⁵Y. Xue, S. Datta, and M. A. Ratner, *Chem. Phys.* **281**, 151 (2002); Y. Xue and M. A. Ratner, *Phys. Rev. B* **68**, 115406 (2003); **68**, 115407 (2003); **69**, 085403 (2004).
- ¹⁶T. Frederiksen, M. Brandbyge, N. Lorente, and A.-P. Jauho, *Phys. Rev. Lett.* **93**, 256601 (2004).
- ¹⁷M. Galperin, A. Nitzan, S. Sek, and M. Majda, *J. Electroanal. Chem.* **550**, 337 (2003).
- ¹⁸H. Haug and A.-P. Jauho, *Quantum Kinetics in Transport and Optics of Semiconductors* (Springer-Verlag, Berlin, 1996); R. Mills, *Propagators for many-particle systems; an elementary treatment* (Gordon and Breach, New York, 1969).
- ¹⁹L. V. Keldysh, *Sov. Phys. J.* **20**, 1018 (1965).
- ²⁰S. Datta, *Electronic Transport in Mesoscopic Systems* (Cambridge University Press, Cambridge, U.K., 1997).
- ²¹M. Schmutz, *Z. Phys. B* **30**, 97 (1978).
- ²²U. Harbola, J. B. Maddox, and S. Mukamel (unpublished).
- ²³O. Berman and S. Mukamel, *Phys. Rev. B* **69**, 155430 (2004).
- ²⁴U. Harbola and S. Mukamel, in *Theory and Applications in Computational Chemistry; The First 40 Years. A Volume of Technical and Historical Perspective*, edited by C. E. Dykstra, G. Frenkin, K. S. Kim, and G. E. Scuseria (Amsterdam, Netherlands, 2005), Chap. 14.
- ²⁵U. Harbola and S. Mukamel, *J. Chem. Phys.* **124**, 1 (2006).
- ²⁶S. Mukamel, *Principles of Nonlinear Optical Spectroscopy* (Oxford University Press, New York, 1995).
- ²⁷Y. Hu and S. Mukamel, *J. Chem. Phys.* **91**, 6973 (1989).
- ²⁸S. Skourtis and S. Mukamel, *Chem. Phys.* **197**, 367 (1995).
- ²⁹S. Mukamel and Y. J. Yan, *Acc. Chem. Res.* **22**, 301 (1989).
- ³⁰C. Cohen-Tannoudji, J. D.-Roc, and G. Grynberg, *Atom-Photon Interactions; Basic Processes and Applications* (Wiley, New York, 1992).

- ³¹V. Chernyak, N. Wang, and S. Mukamel, *Phys. Rep.* **263**, 213 (1995).
- ³²S. Mukamel, *Phys. Rev. E* **68**, 021111 (2003).
- ³³*Coherence and Quantum Optics V*, edited by L. Mandel and E. Wolf (Plenum Press, New York, 1989).
- ³⁴B. R. Mollow, *Theory of Intensity Dependent Resonance Light Scattering and Resonance Fluorescence*, Progress in Optics Vol. XIX, edited by E. Wolf (North-Holland, Amsterdam, 1981), p. 1.
- ³⁵C. Caroli, R. Combescot, P. Nozieres, and D. S.-James, *J. Phys. C* **5**, 21 (1972).
- ³⁶S. Tikhodeev, M. Nataro, K. Makoshi, T. Mii, and H. Ueba, *Surf. Sci.* **493**, 63 (2001).
- ³⁷M. Galperin, M. A. Ratner, and A. Nitzan, *J. Chem. Phys.* **121**, 11965 (2004).
- ³⁸E. K. U. Gross, C. A. Ullrich, and U. J. Gossmann, in *Density Functional Theory*, edited by E. K. U. Gross and R. M. Dreizler, NATO Advanced Study Institute, Series B: Physics (Plenum, New York, 1994); E. K. U. Gross and S. Kurth, in *Relativistic and Electron-Correlation Effects in Molecules and Solids*, edited by G. L. Malli, NATO Advanced Study Institute, Series B: Physics (Plenum, New York, 1993).
- ³⁹G. Onida, L. Reining, and A. Rubio, *Rev. Mod. Phys.* **74**, 601 (2002).
- ⁴⁰F. Aryasetiawan and O. Gunnarsson, *Rep. Prog. Phys.* **61**, 237 (1998).
- ⁴¹M. Wagner, *Phys. Rev. B* **44**, 6104 (1991).
- ⁴²G. D. Mahan, *Many-Particle Physics*, 2nd ed. (Plenum, New York, 1990).
- ⁴³N. Lorente and M. Persson, *Phys. Rev. Lett.* **85**, 2997 (2000).
- ⁴⁴M. J. Frisch *et al.*, computer code. GAUSSIAN 03, rev C.02 (Gaussian, Inc., Wallingford, CT, 2004).
- ⁴⁵J. Tersoff and D. R. Hamann, *Phys. Rev. Lett.* **50**, 1998 (1983).